IOP Publishing
Journal of Physics D: Applied Physics
J. Phys. D: Appl. Phys. **49** (2016) 425204 (22pp)
doi:10.1088/0022-3727/49/42/425204

Air plasma treatment of liquid covered tissue: long timescale chemistry

Amanda M Lietz[1] **and Mark J Kushner**[2]

[1] Department of Nuclear Engineering and Radiological Sciences, University of Michigan, 2355 Bonisteel Blvd., Ann Arbor, MI 48109-2104, USA
[2] Department of Electrical Engineering and Computer Science, University of Michigan, 1301 Beal Ave., Ann Arbor, MI 48109-2122, USA

E-mail: lietz@umich.edu and mjkush@umich.edu

Received 11 July 2016, revised 5 August 2016
Accepted for publication 11 August 2016
Published 22 September 2016

Abstract

Atmospheric pressure plasmas have shown great promise for the treatment of wounds and cancerous tumors. In these applications, the sample is usually covered by a thin layer of a biological liquid. The reactive oxygen and nitrogen species (RONS) generated by the plasma activate and are processed by the liquid before the plasma produced activation reaches the tissue. The synergy between the plasma and the liquid, including evaporation and the solvation of ions and neutrals, is critical to understanding the outcome of plasma treatment. The atmospheric pressure plasma sources used in these procedures are typically repetitively pulsed. The processes activated by the plasma sources have multiple timescales—from a few ns during the discharge pulse to many minutes for reactions in the liquid. In this paper we discuss results from a computational investigation of plasma–liquid interactions and liquid phase chemistry using a global model with the goal of addressing this large dynamic range in timescales. In modeling air plasmas produced by a dielectric barrier discharge over liquid covered tissue, 5000 voltage pulses were simulated, followed by 5 min of afterglow. Due to the accumulation of long-lived species such as ozone and N_xO_y, the gas phase dynamics of the 5000th discharge pulse are different from those of the first pulse, particularly with regards to the negative ions. The consequences of applied voltage, gas flow, pulse repetition frequency, and the presence of organic molecules in the liquid on the gas and liquid reactive species are discussed.

Keywords: atmospheric pressure plasma, plasmas on liquids, dielectric barrier discharges, liquid chemistry, global modeling, air plasma chemistry

(Some figures may appear in colour only in the online journal)

1. Introduction

Atmospheric pressure plasmas (APPs) sustained in air are being investigated in the context of plasma medicine for treating human tissue to promote the healing of wounds [1], especially chronic wounds such as those associated with diabetes. APPs have also been shown to induce apoptosis in cancer cells [2] and to kill bacteria [3–5]. Reactive oxygen and nitrogen species (RONS) represent an important component of the influence of the plasma on biological systems—these species can trigger response pathways in individual cells, as well as produce systemic responses [6]. These RONS consist of radicals such as hydroxyl (OH), hydroperoxyl (HO_2), oxygen atoms (O), nitrogen dioxide (NO_2) and nitric oxide (NO), and other reactive neutrals such as ozone (O_3), singlet delta oxygen ($O_2(^1\Delta_g)$) and peroxynitrous acid (ONOOH). Although several of these reactive species are known to be important in normal biological processes, such as metabolism and response to bacterial invasion [7, 8], the precise mechanisms and roles of these species are not well known.

During plasma treatment, the tissue is often covered by a thin layer of a blood serum-like liquid or a saline-like solution. Plasma produced species are processed by the liquid layer, reacting with each other, the liquid, and organic molecules in the liquid before reaching the underlying tissue. In the case of water dominated liquids, the reaction chemistry of the gas phase plasma–liquid system has multiple timescales. At one extreme are the ns duration processes during the gas phase plasma pulse which produces primary radicals such as O and OH by electron impact dissociation. These species are renewed on a pulse-by-pulse basis. At the other extreme, reactive nitrogen species (RNS) such as HNO_3 accumulate over many tens to thousands of discharge pulses. There are similarly large dynamic ranges of timescales for plasma activated processes in the liquid. For example, solvated OH_{aq} (the aq subscript denotes an aqueous species) reacts on timescales as short as microseconds to form H_2O_{2aq} [9]. In contrast, the density of $ONOOH_{aq}$ may evolve over many hours in plasma activated water [10–12].

The diagnostics available for measuring concentrations of reactive species in liquids are typically limited to long timescales, often minutes and sometimes hours after plasma treatment [13]. Although real-time measurements of selected species are possible, such as for solvated electrons and OH_{aq}, these are not widely applied techniques [14, 15]. Investigations of the plasma activation of liquids may then need to address a large dynamic range in time approaching or exceeding minutes, not only to address the long term chemistry but also to enable comparisons with the available diagnostics.

Several computer models have been developed to address plasma–liquid interactions for biological and environmental investigations. Experiments on the removal of pollutants from a flowing water film by dielectric barrier discharges (DBDs) have been modeled using computational fluid dynamics (CFD) techniques [16]. O_3 and the pollutant were included in this multi-fluid model, while explicitly calculating liquid reactions and pollutant interactions. There was indication that the plasma increased the transport of pollutants from the liquid into the gas, most likely from induced mixing of the liquid. Matsui *et al* developed a model for discharges within O_2 bubbles moving through water [17]. The liquid and gas phase kinetics in this model were weakly coupled. The gas dynamics were solved on different timescales than the liquid and used to update the liquid species. The calculations closely matched experimental measurements of the breakdown of acetic acid by OH. Agreement with the experiments was achieved by including the reaction of O_{aq} with H_2O_{aq}, indicating that this process contributes significantly to OH_{aq} levels in the liquid. A further study separated this system into 3 phases, gas, liquid, and plasma, with each phase represented by global kinetics models [18]. Increasing the water vapor density in the bubble resulted in more H_2O_{2aq} and less O_{3aq}. The water vapor density, and the resulting H_2O_{2aq}, increased as a function of discharge current.

Kelly and Turner developed a model of a radio frequency (RF) plasma jet sustained in He/O_2 while treating the liquid as a reactive surface [19]. The plasma and neutral chemistry were decoupled. Plasma dynamics were resolved as a 1D jet and solved to the steady state. The sources of neutrals based on the plasma dynamics calculations were extrapolated in time for use by a 2D fluid and neutral chemistry model. The treatment of a liquid substrate was considered by assuming a thin layer of gas saturated with water vapor. They showed that H_2O_2, O_3, and $O_2(^1\Delta_g)$ were the dominant RONS in the vapor layer above the liquid, and H_2O_{2aq} would likely be the most abundant RONS in the liquid.

A comprehensive modelling study by Liu *et al* addressed a surface microdischarge sustained remotely from the liquid being treated [20]. The physical domain was divided into 3-zones: plasma, gas consisting of long-lived neutral species, and liquid. The three zones were computationally tightly coupled, and the equations representing the zones were simultaneously integrated. The plasma zone was treated using global kinetics, while the neutral gas and liquid were treated using 1D transport. The most reactive neutral species NO, OH, O, and $O_2(^1\Delta_g)$ did not survive transport from the remote plasma source to the liquid. The most significant gas phase species influencing the liquid chemistry were H_2O_2, O_3, HNO_3, and HNO_2. These species are capable of producing more reactive species in the liquid, such as OH_{aq}, providing a source of reactivity at depths in the liquid that cannot be reached by the more reactive species produced in the remote plasma source.

The goal of the present investigation is to improve our understanding of the influence of operational parameters of atmospheric pressure discharges sustained in air on the chemical activation of liquids, in this case water, on timescales of ns to several minutes. Understanding the coupling of gas phase and liquid chemistry and their dependence on voltage, gas flow, pulse frequency, and the presence of organics in the water is required to optimize the application of these sources for desired biological outcomes. With this goal in mind, in this paper, we discuss results from a computational investigation using a global model of DBD processing of thin water layers for long periods (thousands of discharge pulses) and sufficient post-pulse reaction time that the products in the gas phase and liquid essentially reach their final state.

The importance of multidimensional effects in plasma–liquid interactions is well known. It is true that 2- and 3D models can provide a more complete description of the gas phase breakdown processes, the spatial dependence of the discharge and transport into the liquid. However, the computational burden and complexity of these models make it difficult to address the hundreds to thousands of discharge pulses and many minutes of post-discharge reactions relevant to plasma treated liquids. With the large variety of plasma sources currently being experimentally investigated (e.g. DBDs, surface microdischarges, plasma jets), the parameter space is large. A global model which is capable of addressing both short and long time scales and which is generically applicable to all discharges may provide a viable method to investigate these multiscale processes.

The model employed in this investigation is a global simulation modified to have two 0D zones—one gas phase and one liquid—which exchange species only through the interface between the gas and liquid. Separate reaction mechanisms were employed in each zone. Although this study focuses on the plasma activated liquid chemistry, the chemistry is not the only means through which plasma affects the tissue. High electric fields can initiate electroporation of cell membranes [21], and the role of photons may also be significant, especially as a source of radicals in the liquid by photolysis of water.

We found that for a DBD sustained in humid air, the positive ion dynamics change little over thousands of discharge pulses. However, the negative ion and neutral dynamics evolve as long-lived species such as O_3 and NO_2 accumulate in the gas. In the liquid, many RONS accumulate over thousands of pulses and then decay in the post-plasma period. The pH of the liquid decreases due to the acids (e.g. HNO_x) that are produced in the gas and solvate into the liquid, or are produced directly in the liquid. Increasing voltage increases most of the reactive species densities due to the increase in power deposition. Due to the disparities in timescales for formation of reactive oxygen species (ROS) and RNS, gas flow can be used as a means to regulate the relative rates of solvation of ROS and RNS into the liquid. An increased gas flow rate decreases RNS in the liquid while increasing some ROS. Similarly, pulse repetition frequency (PRF) may be a control mechanism. An increase in PRF increases the ratio of O_{3aq} to HNO_{3aq} produced by the plasma. The presence of organic molecules in the liquid can largely consume the ROS, allowing a larger fluence of RONS to solvate in the liquid for species that normally saturate in the liquid.

The model used in this investigation is described in section 2. Results from this investigation are discussed in section 3. In addition to a detailed analysis of the base case, consequences of varying applied voltage, flow rate, pulse-repetition frequency and organic content of the water are discussed. Concluding remarks are in section 4.

2. Description of the model

The model used in this investigation, *GlobalKin* is a general purpose 0D plasma kinetics model which includes a circuit module, options to address gas flow using plug-flow or residence time approximations, diffusion to surfaces, surface kinetics using a surface site balance model, and most recently, a liquid interactions module [22]. The circuit module provided the current through and voltage across the plasma which results in power deposition. Alternatively, the power deposition in the plasma can be directly specified as a function of time.

An electron energy equation is used for the average electron energy or temperature. Electron energy distributions (EEDs) were obtained from solutions of Boltzmann's equation and were the basis of lookup tables that provided the reaction rate coefficients and transport coefficients of electron impact processes as a function of average energy. These tables were updated at a frequency specified by the user (in this case, at the beginning of each voltage pulse) to reflect the change in these coefficients as the gas mixture evolves. The electron temperature (T_e) was calculated from,

$$\frac{\partial\left(\frac{3}{2}n_e k_b T_e\right)}{\partial t} = \vec{j}\cdot\vec{E} + n_e\sum_i \Delta\varepsilon_i k_i n_i + \sum_i \Delta\varepsilon_i k_i n_{1i} n_{2i} - \sum_i \frac{3}{2} n_e v_{mi}\left(\frac{2m_e}{M_i}\right) k_b (T_e - T_i) \quad (1)$$

where n_e is the electron density and k_b is Boltzmann's constant. The first term on the right-hand-side is the power deposition. All power was assumed to initially be deposited in electrons due to the low mobility of the ions. This assumption is reasonable for the cases considered in this study at atmospheric pressure, but becomes less accurate in low pressure plasmas where significant power is deposited in the sheath by ions. The current density j and the electric field E were obtained from the circuit module. The second term represents changes in electron energy (positive or negative) due to inelastic collisions where $\Delta\varepsilon$ is the change energy during the collision with the species of density n_i for the process having reaction rate coefficient k_i. The third term represents sources of electron energy density due to collisions between gas phase species n_{1i} and n_{2i} and (such as Penning ionizations). The last term represents the electrons transferring momentum to the neutral atoms and molecules through elastic collisions where υ_{mi} is the momentum transfer collision frequency, m_e and M_i are the mass of the electrons and the other species, and T_i is the temperature of the neutral gas.

The density of all gas species was given by

$$\frac{dn_i}{dt} = \sum_j \left\{ (a_{ij}^{(R)} - a_{ij}^{(L)}) k_j \prod_l n_l^{a_{lj}^{(L)}} \right\} + \frac{1}{\tau_{\text{flow}}}\left(n_{io} - n_i\left(1 + \frac{(P - P_0)}{P_0}\right)\right) + \sum_m \left\{ -\frac{D_i n_i}{\Lambda^2} f_m S_{im} + \sum_k \frac{D_k n_k}{\Lambda^2} f_m S_{km} g_{ikm} \right\}. \quad (2)$$

The first term represents the gas phase reactions j which are sources or losses of species i. $a_{ij}^{(R)}$ and $a_{ij}^{(L)}$ are the number of molecules of species i which are on the right hand side and the left hand side of reaction j. The second term represents the sources and losses from flow, where τ_{flow} is the average residence time of the gas in the plasma, n_{io} is the number density of the species flowing into the reactor, P is the instantaneous pressure and P_0 is the desired operating pressure. The pressure dependent term accounts for changes in flow speed that may occur due to increases in pressure resulting from dissociation or gas heating. Diffusion losses including recombination or reactions at the wall are addressed by the third term. The third term includes diffusion losses of species i at the surface of material m and the source due to the return flux after surface reactions occur with other species. f_m is the fractional area of wall material m and D_i is the diffusion coefficient of species i. For charged species this value is their ambipolar diffusion coefficient, and for other species this value is determined by mixture rules using Leonard-Jones potentials. Λ is the diffusion length of the plasma, defined by the geometry of the reactor. The sticking coefficient, S_{km}, is the fraction of the diffusion flux which disappears at the wall, and the give fraction, g_{ikm}, is the fraction of the consumed flux of species k which returns as species i.

The gas temperature was calculated by

$$\begin{aligned}\frac{\mathrm{d}\left(\frac{3}{2}N_{\mathrm{g}}c_{\mathrm{p}}T_{\mathrm{g}}\right)}{\mathrm{d}t} &= P_{\mathrm{ion}} + \sum_i \frac{3}{2}n_{\mathrm{e}}\nu_{\mathrm{m}i}\left(\frac{2m_{\mathrm{e}}}{M_i}\right)k_{\mathrm{b}}(T_{\mathrm{e}} - T_i) \\ &+ \sum_i \Delta\varepsilon_i^{\mathrm{fc}}R_i - \sum_i \Delta H_i R_i \\ &+ \frac{1}{\tau_{\mathrm{flow}}}\left(N_{\mathrm{g}0}c_{\mathrm{p}0}T_{\mathrm{g}0} - N_{\mathrm{g}}c_{\mathrm{p}}T_{\mathrm{g}}\left(\frac{P}{P_0}\right)\right) \\ &- \frac{\kappa}{\Lambda^2}(T_{\mathrm{g}} - T_{\mathrm{w}}) \qquad (3)\end{aligned}$$

where N_{g} is the total gas density, c_{p} is the specific heat of the gas, and T_{g} is the gas temperature. P_{ion} is the power deposited into the ions by the ambipolar electric field. The second term is the gas heating due to elastic collisions between the electrons and all other species. Franck–Condon heating is captured by the third term, where $\Delta\varepsilon_i^{\mathrm{fc}}$ is the energy released as gas heating in dissociation reactions and R_i is the rate of reaction i. The fourth term includes the change in enthalpy from all reactions, including charge exchange, where ΔH_i is the change in enthalpy of reaction i, and R_i is the reaction rate. The fifth term is advective cooling due to gas flow, where $N_{\mathrm{g}0}$, $c_{\mathrm{p}0}$, and $T_{\mathrm{g}0}$, are the density, specific heat, and temperature of the gas flowing into the reactor. P_0 is the set-point pressure, and P is the current pressure. The last term addresses thermal conduction to surfaces, where κ is the thermal conductivity, and T_{w} is the surface or wall temperature.

2.1. Liquid module

To address the plasma activation of a liquid layer in contact with the plasma, a second set of species and a separate reaction mechanism were included in the global model. First, a duplicate solvated species was added for each gas phase species (i.e. $H_2O_{2\mathrm{aq}}$ was added for H_2O_2). The liquid-resident species and reaction mechanism are restricted to a second zone in the model. The species in these two zones (gas and liquid) only interact through the interface between the zones by means of diffusion into or out of the liquid. Conceptually, the gas–liquid interface is treated as one of the materials to which species diffuse and so is mechanically included in the sum of materials in equation (2). For the material that represents the gas–liquid interface, the sticking coefficient for the diffusion losses of neutral species from the gas to the liquid is determined by the Henry's law equilibrium constant, h_i. For species i and liquid material m,

$$S_{im} = \frac{h_i n_{i,\mathrm{g}} - n_{i,\mathrm{l}}}{h_i n_{i,\mathrm{g}}} \qquad (4)$$

where $n_{i,\mathrm{g}}$ is the gas phase density of species i and $n_{i,\mathrm{l}}$ is its liquid phase density. This sticking coefficient is used for $n_{i,\mathrm{l}}/n_{i,\mathrm{g}} < h_i$ and accounts for a diminishing rate of loss of the gas phase species into the liquid as the liquid density approaches its Henry's law equilibrium values. If $n_{i,\mathrm{l}}/n_{i,\mathrm{g}} > h_i$ at any time, then the liquid is oversaturated and transport of the species is from the liquid into the gas. The flux from the oversaturated liquid to the gas is given by:

$$\Gamma_i = \frac{D_i(n_{i,\mathrm{l}} - h_i n_{i,\mathrm{g}})}{\Lambda^2}\frac{V_{\mathrm{p}}}{A_{\mathrm{l}}} \qquad (5)$$

where V_{p} is the volume of the plasma region and A_{l} is the surface area of the face representing the gas–liquid interface. Once a species enters the liquid, transport in the liquid phase is assumed to be well stirred [23, 24]. In making this assumption, the global model does not capture formation of a boundary layer in the liquid at each pulse which may saturate.

Table 1. Henry's law constants ([25]).

Species	h (unitless)	Note
H_2O_2	1.92×10^6	
HO_2	1.32×10^5	
OH	6.20×10^2	
H	6.48×10^3	
H_2	1.80×10^{-2}	
O, O(^1D)	1	[a,b]
O_2, $O_2(v)$, $O_2(^1\Delta_g)$, $O_2(^1\Sigma_u)$	3.24×10^{-2}	[a]
O_3	3.00×10^{-1}	
N_2, $N_2(A^3\Sigma_u)$, $N_2(v)$, N, N(^2D), $N_2(a'^1\Sigma)$	1.60×10^{-2}	[a]
N_2O_3	6.00×10^2	
N_2O_4	3.69×10^1	
N_2O_5	4.85×10^1	
N_2O	5.99×10^{-1}	
HO_2NO_2	2.99×10^5	
NO	4.40×10^{-2}	
NO_2	2.80×10^{-1}	
NO_3	4.15×10^1	
HNO_2, HNO	1.15×10^3	[a]
HNO_3, ONOOH	4.80×10^6	
CO, CO(v)	2.42×10^{-2}	[a]
CO_2, $CO_2(v)$	8.23×10^{-1}	[a]
NH	1.47×10^3	[c]

[a] Value corresponds to the first species in the list. Other species were assumed to have the same Henry's law constant.

[b] Approximated. Species reacts quickly in water and will not reach Henry's law saturation.

[c] Approximated by analogy to NH_3.

The liquid species densities are given by

$$\begin{aligned}\frac{\mathrm{d}n_i}{\mathrm{d}t} &= \sum_j \left\{(a_{ij}^{(\mathrm{R})} - a_{ij}^{(\mathrm{L})})k_j \prod_l n_l^{a_{lj}^{(\mathrm{L})}}\right\} + \frac{D_i n_{i,\mathrm{g}}}{\Lambda^2} f_{\mathrm{l}} S_{i,\mathrm{liquid}} \frac{V_{\mathrm{p}}}{V_{\mathrm{l}}} \\ &- \max\left\{0, \frac{D_i(n_{i,\mathrm{l}} - h_i n_{i,\mathrm{g}})}{\Lambda^2}\frac{V_{\mathrm{p}}}{V_{\mathrm{l}}}\right\} \qquad (6)\end{aligned}$$

where n_i is the density of the liquid species i. The first term represents the liquid phase reactions j which are sources or losses of species i. $a_{ij}^{(\mathrm{R})}$ and $a_{ij}^{(\mathrm{L})}$ are the number of molecules of species i which is on the right hand side and the left hand side of reaction j. k_j is the reaction rate coefficient of reaction j. The second term represents diffusion of species from the gas into the liquid, where D_i is the diffusion coefficient of gas phase species i, $n_{i,\mathrm{g}}$ is the density of species i in the gas, Λ is the diffusion length of the plasma, defined by the geometry. $S_{i,\mathrm{l}}$, is the sticking coefficient of species i on the liquid and f_{l} is the fraction of the area of the plasma which is in contact with the liquid V_{p} and V_{l} are the volumes of the plasma and liquid region. The third term represents transport out of the liquid when the liquid is oversaturated. This term is only nonzero when the liquid is oversaturated, and it represents the flux in equation (5).

With liquid in contact with the gas, evaporation of the liquid into the gas phase is included in equation (2) to account for, for example, humidifying the gas. The flux into the gas phase due to evaporation increases the density of the vapor phase but the evaporation losses of mass from the liquid are ignored, as they are assumed to be much smaller than the total liquid volume. The evaporating flux is

$$\Gamma_{i,\mathrm{e}} = \frac{D_i(n_{i,\mathrm{s}} - n_{i,\mathrm{g}})}{\Lambda^2}\frac{V_\mathrm{p}}{A_\mathrm{l}} \tag{7}$$

where $n_{i,\mathrm{s}}$ is the gas number density corresponding to the saturated vapor pressure of the liquid.

2.2. Reaction mechanism

The full reaction mechanism contains 79 gas phase species, 83 liquid phase species, 1680 gas phase reactions, and 448 liquid reactions. The mechanism includes the species associated with a humid air plasma interacting with water. Henry's law constants used in the model are listed in table 1. In large part, the gas phase reaction mechanism developed by Van Gaens *et al* [26] for argon atmospheric pressure plasma jets interacting with humid air was used for the gas phase portion of the mechanism with the addition of carbon dioxide (CO_2).

The liquid mechanism, shown in table 2, is based on that of Tian *et al* [27] with modifications to address all species in the gas phase mechanism and some improvements based on recent publications. Water cluster ions were added to the gas phase mechanism and assumed to charge exchange with water on timescales of several ns. In particular, the peroxynitrite chemistry has been improved based on recent experiments [10]. For each weak acid hydrolysis reaction, the reverse process was also added with an appropriate rate coefficient to fit with the dissociation constant for each acid. These updates enable a better estimate of the pH in the liquid. Long timescale decay reactions were added to address the many minutes studied here, including the thermal decay of peroxynitrite, ozone, $O_2(^1\Delta_g)$, and the ozone anion. Several excited states from the gas phase mechanism were added to the liquid mechanism. The liquid reactivity in this reaction mechanism may be overestimated, as excited states from the gas phase entering the liquid with enough energy to dissociate H_2O were assumed to perform that dissociation. In reality there is some branching ratio between dissociative and non-dissociative deexcitation.

2.3. Geometry and operational parameters

The discussion of results from this investigation is organized into several sections—base case, varying voltage, flow rate of gases, pulse repetition frequency, and presence of biomolecules in the liquid. In all cases the geometry is as shown in figure 1, and represents treatment of tissue having an area of 1 cm^2 covered by 1 mm of water, with an air gap of 2 mm. The simulation is initialized with humid air at 100% relative humidity ($N_2/O_2/H_2O/CO_2 = 76.6/20.3/3.5/0.03$) as would

Table 2. Aqueous reaction mechanism.

Reaction	Rate coefficient[a]	Ref.
Ions		
$e_{aq} + H_2O_{aq} \rightarrow H_2O^-_{aq}$	5×10^{-15}	[b]
$M^+_{aq} + H_2O_{aq} \rightarrow H_2O^+_{aq} + M_{aq}$, $M^+_{aq} = N^+_{2aq}, N^+_{aq}, O^+_{2aq}, NO^+_{aq}, H^+_{2aq}, NO^+_2, CO^+_{2aq}, CO^+_{aq}$	5×10^{-15}	[b]
$N^+_{4aq} + H_2O_{aq} \rightarrow H_2O^+_{aq} + N_{2aq} + N_{2aq}$	5×10^{-15}	[b]
$O^+_{4aq} + H_2O_{aq} \rightarrow H_2O^+_{aq} + O_{2aq} + O_{2aq}$	5×10^{-15}	[b]
$H^+_{aq} + H_2O_{aq} \rightarrow H_3O^+_{aq}$	5×10^{-15}	[b]
$N^+_{3aq} + H_2O_{aq} \rightarrow H_2O^+_{aq} + N_{2aq} + N_{aq}$	5×10^{-15}	[b]
$H_2O^+_{aq} + H_2O_{aq} \rightarrow H_3O^+_{aq} + OH_{aq}$	1×10^{-17}	[28]
$H^-_{aq} + H_2O_{aq} \rightarrow H_2O^-_{aq} + H_{aq}$	5×10^{-15}	[b]
$H_2O^-_{aq} + H_2O_{aq} \rightarrow H_{aq} + OH^-_{aq} + H_2O_{aq}$	3×10^{-20}	[28]
$O^-_{aq} + H_2O_{aq} \rightarrow OH^-_{aq} + OH_{aq}$	3×10^{-15}	[29]
Cluster ions		
$M^+(H_2O)_{naq} \rightarrow M^+_{aq} + nH_2O_{aq}$, $M^+_{aq} = H_3O^+_{aq}, H_2O^+_{aq}, NO^+_{aq}, O^+_{2aq}, N^+_{aq}$	$1.68 \times 10^8\ \mathrm{s}^{-1}$	[b]
$M^-(H_2O)_{aq} \rightarrow M_{aq} + H_2O^-_{aq} + (n-1)\ H_2O_{aq}$, $M^-_{aq} = O^-_{2aq}, O^-_{aq}, OH^-_{aq}$	$1.68 \times 10^8\ \mathrm{s}^{-1}$	[b]
$NO^+O_2 \rightarrow NO^+_{aq} + O_{2aq}$	$1.68 \times 10^8\ \mathrm{s}^{-1}$	[b]
Electronic and vibrational excited states		
$N_2(v)_{aq} + H_2O_{aq} \rightarrow N_{2aq} + H_2O_{aq}$	5×10^{-15}	[b]
$N(^2D)_{aq} + H_2O_{aq} \rightarrow NH_{aq} + OH_{aq}$	6.9×10^{-39}	[30][c]
$N(^2D)_{aq} + H_2O_{aq} \rightarrow N_{aq} + H_2O_{aq}$	2.4×10^{-14}	[31][c]
$N_2(a'^1\Sigma)_{aq} + H_2O_{aq} \rightarrow OH_{aq} + H_{aq} + N_{2aq}$	5×10^{-15}	[b]
$O_2(v)_{aq} + H_2O_{aq} \rightarrow O_{2aq} + H_2O_{aq}$	5×10^{-15}	[b]
$O_2(^1\Sigma_u)_{aq} + H_2O_{aq} \rightarrow O_{2aq} + H_2O_{aq}$	5×10^{-15}	[b]
$O(^1D)_{aq} + H_2O_{aq} \rightarrow O_{aq} + H_2O_{aq}$	1.2×10^{-11}	[31][c]
$O_2(^1\Delta_g)_{aq} + H_2O_{aq} \rightarrow O_{2aq} + H_2O_{aq}$	7.7×10^{-18}	[32][c]
$N_2(A^3\Sigma_u)_{aq} + H_2O_{aq} \rightarrow N_{2aq} + H_2O_{aq}$	1×10^{-10}	[b]
$N_2(A^3\Sigma_u)_{aq} + H_2O_{aq} \rightarrow N_{2aq} + OH_{aq} + H_{aq}$	6×10^{-14}	[30][c]
Acid dissociation		
$ONOOH_{aq} + H_2O_{aq} \rightarrow H_3O^+_{aq} + ONOO^-_{aq}$	5×10^{-15}	[b]
$ONOO^-_{aq} + H_3O^+_{aq} \rightarrow H_2O_{aq} + ONOOH_{aq}$	1.75×10^{-6}	[d]
$HO_{2aq} + H_2O_{aq} \rightarrow H_3O^+_{aq} + O^-_{2aq}$	1.43×10^{-17}	[d]
$H_3O^+_{aq} + O^-_{2aq} \rightarrow HO_{2aq} + H_2O_{aq}$	5×10^{-11}	[b]
$HNO_{2aq} + H_2O_{aq} \rightarrow H_3O^+_{aq} + NO^-_{2aq}$	5×10^{-15}	[b]
$H_3O^+_{aq} + NO^-_{2aq} \rightarrow H_{aq} + HO_{2aq} + H_2O_{aq}$	6.81×10^{-10}	[d]
$HNO_{3aq} + H_2O_{aq} \rightarrow H_3O^+_{aq} + NO^-_{3aq}$	3×10^{-18}	[33][d]
$H_3O^+_{aq} + NO^-_{3aq} \rightarrow HNO_{3aq} + H_2O_{aq}$	7×10^{-16}	[d]
$HO_2NO_{2aq} + H_2O_{aq} \rightarrow O_2NO^-_{2aq} + H_3O^+_{aq}$	5×10^{-15}	[b]
$O_2NO^-_{2aq} + H_3O^+_{aq} \rightarrow HO_2NO_{2aq} + H_2O_{aq}$	1.05×10^{-7}	[d]
Reactive oxygen species (ROS)		
$OH_{aq} + H_{aq} \rightarrow H_2O_{aq}$	3×10^{-11}	[29]
$H_2O^-_{aq} + H_{aq} \rightarrow H_{2aq} + OH^-_{aq}$	4×10^{-11}	[28]
$H_2O^-_{aq} + O_{aq} \rightarrow O^-_{aq} + H_2O_{aq}$	3×10^{-11}	[29]
$H_2O^-_{aq} + O_{2aq} \rightarrow O^-_{2aq} + H_2O_{aq}$	3×10^{-11}	[28]
$H_2O^-_{aq} + OH_{aq} \rightarrow OH^-_{aq} + H_2O_{aq}$	5×10^{-11}	[28]
$H_2O^-_{aq} + H_2O_{2aq} \rightarrow OH_{aq} + OH^-_{aq} + H_2O_{aq}$	2×10^{-11}	[28]
$H_2O^-_{aq} + O^-_{aq} \rightarrow OH^-_{aq} + OH^-_{aq}$	2×10^{-11}	[28]

(*Continued*)

Table 2. (*Continued*)

Reaction	Rate coefficient[a]	Ref.
$H_2O^-_{aq} + HO^-_{2aq} \rightarrow OH^-_{aq} + OH^-_{aq} + OH_{aq}$	5×10^{-12}	[28]
$H_2O^-_{aq} + H_2O^-_{aq} \rightarrow H_{2aq} + OH^-_{aq} + OH^-_{aq}$	1×10^{-11}	[28]
$H_3O^+_{aq} + OH^-_{aq} \rightarrow H_{aq} + OH_{aq} + H_2O_{aq}$	1×10^{-10}	[29]
$H_2O_{aq} \rightarrow H_2O^+_{aq} + e_{aq}$	1×10^{-20} s^{-1}	[f]
$H_2O_{aq} \rightarrow OH_{aq} + H$	1×10^{-20} s^{-1}	[30][c,f]
$OH_{aq} + H_{aq} \rightarrow H_2O_{aq}$	3×10^{-11}	[29]
$H_2O^-_{aq} + H_2O^+_{aq} \rightarrow H_{aq} + OH_{aq} + H_2O_{aq}$	1×10^{-9}	[28]
$OH_{aq} + OH_{aq} \rightarrow H_2O_{2aq}$	1.7×10^{-11}	[28]
$OH_{aq} + H_{2aq} \rightarrow H_{aq} + H_2O_{aq}$	6×10^{-14}	[28]
$OH_{aq} + HO_{2aq} \rightarrow O_{2aq} + H_2O_{aq}$	2×10^{-11}	[29]
$OH_{aq} + H_2O_{2aq} \rightarrow HO_{2aq} + H_2O_{aq}$	1×10^{-13}	[29]
$OH_{aq} + OH^-_{aq} \rightarrow O^-_{aq} + H_2O_{aq}$	8×10^{-12}	[29]
$OH_{aq} + O^-_{aq} \rightarrow HO^-_{2aq}$	4×10^{-11}	[28]
$OH_{aq} + O^-_{2aq} \rightarrow O_{2aq} + OH^-_{aq}$	1.5×10^{-11}	[28]
$OH_{aq} + HO^-_{2aq} \rightarrow HO_{2aq} + OH^-_{aq}$	1.5×10^{-11}	[28]
$H_{aq} + H_2O_{aq} \rightarrow H_{2aq} + OH_{aq}$	1.5×10^{-21}	[29]
$H_{aq} + H_{aq} \rightarrow H_{2aq}$	1.5×10^{-11}	[29]
$H_{aq} + OH^-_{aq} \rightarrow H_2O^-_{aq}$	3×10^{-14}	[28]
$H_{aq} + HO_{2aq} \rightarrow H_2O_{2aq}$	3×10^{-11}	[28]
$H_{aq} + H_2O_{2aq} \rightarrow OH_{aq} + H_2O_{aq}$	1.5×10^{-13}	[28]
$H_{2aq} + H_2O_{2aq} \rightarrow H_{aq} + OH_{aq} + H_2O_{aq}$	1×10^{-14}	[28]
$H^-_{aq} + H_2O^+_{aq} \rightarrow H_{aq} + H_2O_{aq}$	3×10^{-6}	[34][g]
$H^-_{aq} + H_3O^+_{aq} \rightarrow H_{2aq} + H_2O_{aq}$	3×10^{-6}	[34][g]
$O_{aq} + H_2O_{aq} \rightarrow OH_{aq} + OH_{aq}$	2.2×10^{-17}	[28][h]
$O_{aq} + O_{2aq} \rightarrow O_{3aq}$	5×10^{-12}	[29]
$O_{2aq} + H_{aq} \rightarrow HO_{2aq}$	5×10^{-11}	[28]
$O^-_{aq} + H_{2aq} \rightarrow H_{aq} + OH^-_{aq}$	1.3×10^{-13}	[28]
$O^-_{aq} + O_{2aq} \rightarrow O^-_{3aq}$	5×10^{-12}	[28]
$O^-_{aq} + H_2O_{2aq} \rightarrow O^-_{2aq} + H_2O_{aq}$	8×10^{-13}	[28]
$O^-_{aq} + HO^-_{2aq} \rightarrow O^-_{2aq} + OH^-_{aq}$	8×10^{-13}	[28]
$O(^1D)_{aq} + H_2O_{aq} \rightarrow H_{2aq} + O_{2aq}$	2.3×10^{-12}	[30][c]
$O(^1D)_{aq} + H_2O_{aq} \rightarrow OH_{aq} + OH_{aq}$	2.2×10^{-10}	[30][c]
$O(^1D)_{aq} + O_{2aq} \rightarrow O_{aq} + O_{2aq}$	3.8×10^{-11}	[30][c]
$O(^1D)_{aq} + O_{3aq} \rightarrow O_{2aq} + O_{aq} + O_{aq}$	1.2×10^{-10}	[30][c]
$O(^1D)_{aq} + O_{3aq} \rightarrow O_{2aq} + O_{2aq}$	5.04×10^{-10}	[30][c]
$O(^1D)_{aq} + N_2O_{aq} \rightarrow NO_{aq} + NO_{aq}$	6.7×10^{-11}	[30][c]
$O^-_{3aq} + OH_{aq} \rightarrow O^-_{2aq} + HO_{2aq}$	1.41×10^{-11}	[29]
$O^-_{3aq} + O^-_{aq} \rightarrow O^-_{2aq} + O^-_{2aq}$	1.7×10^{-13}	[29]
$O^-_{3aq} + H_3O^+_{aq} \rightarrow O_{2aq} + OH_{aq} + H_2O_{aq}$	1.50×10^{-10}	[29]
$O^-_{3aq} \rightarrow O_{2aq} + O^-_{aq}$	2.6×10^{3} s^{-1}	[29]
$O^-_{2aq} + HO_{2aq} + H_2O_{aq} \rightarrow O_{2aq} + H_2O_{2aq} + OH^-_{aq}$	2.68×10^{-34} cm^6 s^{-1}	[29]
$O^-_{2aq} + H_2O_{2aq} \rightarrow O_{2aq} + OH_{aq} + OH^-_{aq}$	2.16×10^{-22}	[29]
$O^-_{2aq} + O^-_{aq} + H_2O_{aq} \rightarrow O_{2aq} + OH^-_{aq} + OH^-_{aq}$	2.98×10^{-35} cm^6 s^{-1}	[29]
$O_{3aq} \rightarrow O_{2aq} + O_{aq}$	3×10^{-6} s^{-1}	[29]
$O^+{}_{aq} + H_2O_{aq} \rightarrow H_2O^+_{aq} + O_{aq}$	1.2×10^{-12}	[31][c]
$O^+{}_{aq} + O_{2aq} \rightarrow O^+_{2aq} + O_{aq}$	1.9×10^{-11}	[35][c]
$O_{3aq} + OH^-_{aq} \rightarrow O^-_{2aq} + HO_{2aq}$	1.16×10^{-19}	[29]
$O_{3aq} + O^-_{2aq} \rightarrow O^-_{3aq} + O_{2aq}$	2.66×10^{-12}	[29]
Reactive nitrogen species (RNS)		
$N_{aq} + N_{aq} \rightarrow N_{2aq}$	5×10^{-14}	[30][c]
$N_{aq} + H_2O_{aq} \rightarrow NH_{aq} + OH_{aq}$	6.93×10^{-39}	[30][c]
$H_{aq} + HNO_{aq} \rightarrow OH_{aq} + NH_{aq}$	2.18×10^{-22}	[30][c]
$NH_{aq} + NO_{aq} \rightarrow N_2O_{aq} + H_{aq}$	1.3×10^{-12}	[30][c]
$NH_{aq} + O_{2aq} \rightarrow HNO_{aq} + O_{aq}$	2.3×10^{-13}	[31][c]
$O^+_{aq} + N_{2aq} \rightarrow NO^+_{aq} + N_{aq}$	1.2×10^{-12}	[31][c]
$OH_{aq} + NO^-_{2aq} \rightarrow OH^-_{aq} + NO_{2aq}$	1.7×10^{-11}	[29]
$H_{aq} + NO^-_{2aq} \rightarrow NO_{aq} + OH^-_{aq}$	2×10^{-12}	[29]
$O^-_{aq} + NO^-_{2aq} + H_2O_{aq} \rightarrow NO_{2aq} + OH^-_{aq} + OH^-_{aq}$	1.82×10^{-35} cm^6 s^{-1}	[29]
$O^-_{2aq} + NO_{aq} \rightarrow NO^-_{3aq}$	6×10^{-12}	[29]
$NO_{2aq} + NO_{2aq} + H_2O_{aq} + H_2O_{aq} \rightarrow H_3O^+_{aq} + NO^-_{3aq} + HNO_{2aq}$	1.26×10^{-56} cm^9 s^{-1}	[29]
$NO_{2aq} + NO_{2aq} + H_2O_{aq} + H_2O_{aq} + H_2O_{aq} \rightarrow H_3O^+_{aq} + NO^-_{3aq} + H_3O^+_{aq} + NO^-_{2aq}$	1.30×10^{-79} cm^{12} s^{-1}	[29]
$NO_{aq} + NO_{aq} + O_{2aq} \rightarrow NO_{2aq} + NO_{2aq}$	6.28×10^{-36} cm^6 s^{-1}	[29]
$NO_{aq} + NO_{2aq} + H_2O_{aq} \rightarrow HNO_{2aq} + HNO_{2aq}$	5.55×10^{-34} cm^6 s^{-1}	[29]
$NO_{3aq} + H_2O_{aq} \rightarrow HNO_{3aq} + OH_{aq}$	4.8×10^{-14}	[29]
$NO_{aq} + HO_{2aq} \rightarrow HNO_{3aq}$	5.33×10^{-12}	[29]
$NO_{2aq} + H_{aq} \rightarrow HNO_{2aq}$	1.67×10^{-11}	[29]
$OH_{aq} + NO_{aq} \rightarrow HNO_{2aq}$	3.3×10^{-11}	[33]
$OH_{aq} + NO_{2aq} \rightarrow HNO_{3aq}$	2×10^{-11}	[33]
$OH_{aq} + HNO_{3aq} \rightarrow NO_{3aq} + H_2O_{aq}$	2.17×10^{-13}	[29]
$H_{aq} + HNO_{2aq} \rightarrow NO_{aq} + H_2O_{aq}$	7.5×10^{-13}	[29]
$O_{2aq} + NO_{aq} + NO_{aq} \rightarrow NO_{2aq} + NO_{2aq}$	7.7×10^{-36} cm^6 s^{-1}	[29]
$N_2O_{3aq} + H_2O_{aq} \rightarrow HNO_{2aq} + HNO_{2aq}$	1.93×10^{-17}	[30][c]
$N_2O_{4aq} + H_2O_{aq} \rightarrow HNO_{2aq} + HNO_{3aq}$	1.33×10^{-18}	[30][c]
$N_2O_{5aq} + H_2O_{aq} \rightarrow NO_{2aq} + NO_{3aq} + H_2O_{aq}$	1.4×10^{-19}	[30][c]
$N_2O_{5aq} + H_2O_{aq} \rightarrow HNO_{3aq} + HNO_{3aq}$	2×10^{-21}	[30][c]
$NO^-_{2aq} + O_{3aq} \rightarrow NO^-_{3aq} + O_{2aq}$	6.15×10^{-16}	[29]
$N_2O_{5aq} + H_2O_{aq} \rightarrow ONOOH_{aq} + ONOOH_{aq}$	2×10^{-21}	[30][c]
$NO_{aq} + HO_{2aq} \rightarrow ONOOH_{aq}$	5.33×10^{-12}	[29]
$NO_{2aq} + OH_{aq} \rightarrow ONOOH_{aq}$	1.99×10^{-11}	[10]
$H_2O_{2aq} + NO^-_{2aq} + H_3O^+_{aq} \rightarrow ONOOH_{aq} + H_2O_{aq} + H_2O_{aq}$	3.04×10^{-39} cm^6 s^{-1}	[10]
$ONOOH_{aq} + H_2O_{aq} \rightarrow H_3O_{aq} + NO^-_{3aq}$	2.9×10^{-23}	[10]
$ONOOH_{aq} + H_2O_{aq} \rightarrow OH_{aq} + NO_{2aq} + H_2O_{aq}$	1.24×10^{-23}	[10]
$NO_{aq} + O^-_{2aq} \rightarrow ONOO^-_{aq}$	7.14×10^{-12}	[10]
$HNO_{aq} + O_{2aq} \rightarrow HO_{2aq} + NO_{aq}$	8.01×10^{-21}	[30][c]
$HNO_{aq} + O_{3aq} \rightarrow O_{2aq} + HNO_{2aq}$	9.61×10^{-15}	[30][c]
$HNO_{aq} + OH_{aq} \rightarrow H_2O_{aq} + NO_{aq}$	8.00×10^{-11}	[30][c]
$OH_{aq} + N_2O_{aq} \rightarrow HNO_{aq} + NO_{aq}$	3.8×10^{-17}	[31][c]
$NO^-_{2aq} + N_2O_{aq} \rightarrow NO^-_{3aq} + N_{2aq}$	5×10^{-13}	[31][c]
$O_2NO^-_{2aq} \rightarrow NO^-_{2aq} + O_{2aq}$	1 s^{-1}	[29]

(*Continued*)

Table 2. *(Continued)*

Reaction	Rate coefficient[a]	Ref.
$HO_2NO_{2aq} + HNO_{2aq} \rightarrow HNO_{3aq} + HNO_{3aq}$	1.99×10^{-20}	[29]
$HO_2NO_{2aq} \rightarrow HNO_{2aq} + O_{2aq}$	$7 \times 10^{-4}\ s^{-1}$	[29]
$HO_2NO_{2aq} \rightarrow HO_{2aq} + NO_{2aq}$	$4.6 \times 10^{-3}\ s^{-1}$	[29]
CO_x		
$CO_{2aq} + H_{aq} \rightarrow CO_{aq} + OH_{aq}$	1.4×10^{-29}	[30][c]
$CO_{2aq} + O_{aq} \rightarrow CO_{aq} + O_{2aq}$	1.2×10^{-49}	[30][c]
$CO_{2aq} + M_{aq} \rightarrow CO_{aq} + O_{aq} + M$	3.2×10^{-90}	[30][c]
$CO_{2aq} + O(^1D)_{aq} \rightarrow O_{2aq} + CO_{aq}$	2×10^{-10}	[30][c]
$CO_{2aq} + O(^1D)_{aq} \rightarrow O_{aq} + CO_{2aq}$	2.5×10^{-10}	[30][c]
$CO_{2aq} + O_2(^1\Delta_g)_{aq} \rightarrow O_{2aq} + CO_{2aq}$	3×10^{-18}	[30][c]
$CO_2(v)_{aq} + M_{aq} \rightarrow CO_{aq} + M_{aq}$	1×10^{-13}	[36][c,i]
$CO_{aq} + H_2O_{aq} \rightarrow CO_{2aq} + H_{2aq}$	1.72×10^{-13}	[37][c]
$OH_{aq} + CO_{aq} \rightarrow CO_{2aq} + H_{aq}$	1.2×10^{-13}	[30][c]
$CO_{aq} + O_{2aq} \rightarrow CO_{2aq} + O_{aq}$	7.6×10^{-47}	[30][c]
$CO_{aq} + HO_{2aq} \rightarrow OH_{aq} + CO_{2aq}$	1.5×10^{-27}	[30][c]
$CO_{aq} + NO_{2aq} \rightarrow CO_{2aq} + NO_{aq}$	4.44×10^{-35}	[30][c]
$CO_{aq} + O_{3aq} \rightarrow O_{2aq} + CO_{2aq}$	4×10^{-25}	[30][c]
$CO(v)_{aq} + M_{aq} \rightarrow CO_{aq} + M_{aq}$	1×10^{-14}	[36][c,i]
$O(^1D)_{aq} + CO_{2aq} \rightarrow O_{2aq} + CO_{aq}$	2×10^{-10}	[30][c]
$O(^1D)_{aq} + CO_{2aq} \rightarrow O_{aq} + CO_{2aq}$	2.5×10^{-10}	[30][c]
$O^+_{aq} + CO_{2aq} \rightarrow CO^+_{2aq} + O_{aq}$	1×10^{-9}	[31][c]

[a] Aqueous species have an 'aq'. Rate coefficients are for 300 K and have units of $cm^3\ s^{-1}$ unless noted otherwise. $1\ cm^3\ s^{-1} = 6.02 \times 10^{20}\ M^{-1}\ s^{-1}$.

[b] The solvation rate coefficient was estimated to be faster than other liquid reactions in order to not be rate limiting.

[c] Approximated by analogy to gas phase reactions.

[d] Estimated based on the rate of the reverse reaction and the pK_a.

[e] The rate coefficient is estimated according to thermodynamic hydrolysis in liquid water.

[f] Actual rate is lower, rate is negligible in both cases.

[g] Based on a general ion-ion recombination rate.

[h] Approximated by analogy.

[i] Approximated based on measured *V-T* relaxation time.

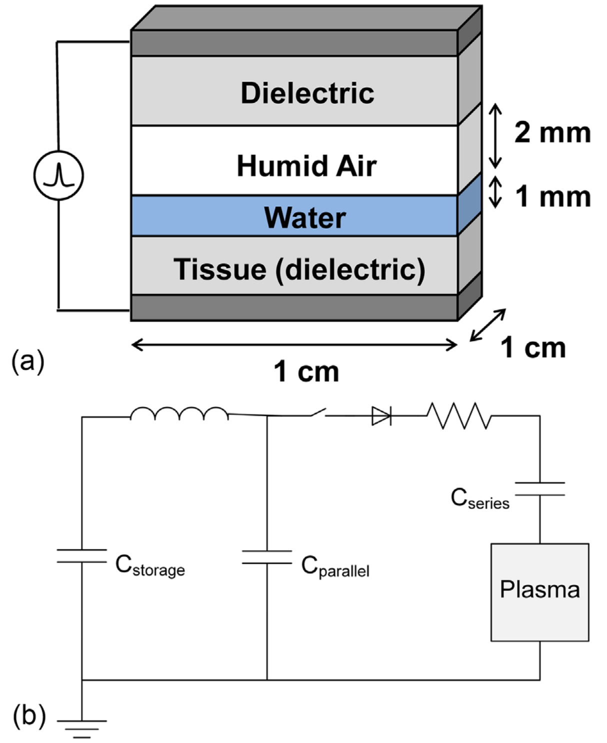

Figure 1. Model parameters. (a) The geometry used in the model. The area being treated is $1\ cm^2$. (b) The circuit applied to the DBD in the model. The values of each circuit element are $C_{storage} = 200$ nF, $R = 1\ \Omega$, $L = 100$ nH, and $C_{series} = C_{parallel} = 1$ pF. C_{series} in the circuit includes the capacitance of the dielectric, the water layer, and the tissue. The storage capacitor is charged to the line voltage at the beginning of each pulse, and the circuit module turns off after the current switches polarities.

occur over several minutes of exposure of the narrow gas gap to the liquid surface. The exception is when varying gas flow, where the initial humidity is 50% to reflect the incoming gas from the ambient. The liquid in the base case is pure water with 8.9 ppm dissolved N_2, 4.8 ppm dissolved O_2, and 140 ppb CO_2, which are their equilibrium values with air. The diffusion length in the gas phase is $d/\pi = 637\ \mu m$, where d is the width of the air gap. In the base case, the applied voltage is 10 kV, at a PRF of 500 Hz. The simulation is run for 5000 pulses (10 s) followed by a 290 second post-pulse period (5 min total). By holding the top surface and tissue at 300 K, there is no significant gas heating in the base case.

The circuit addressed in the model is shown in figure 1(b). The capacitance of the water in the circuit model is 71 pF, and the total series capacitance, due to the liquid and the tissue, is 1 pF. The circuit then consists of a capacitor (1 pF) and resistance (1 Ω) in series with the plasma, a capacitor in parallel with the plasma (1 pF), and a switch having an inductance of (100 nH). A constant voltage is applied by assuming that the storage capacitor ($C_{storage}$) is initially at the applied voltage. The storage capacitance is much greater than the parallel and series capacitance, so its charge is not depleted during the discharge pulse. The switch is closed at the beginning of each pulse. The circuit module turns off when the voltage across the plasma changes polarities, and is kept off until the beginning of the next pulse. All of the circuit parameters are reset with each pulse. The initial charge on the series capacitor is set to zero, the initial current is assumed to be zero, and the discharge voltage is set to 10 kV. At the beginning of each pulse the electron density is renormalized to be at least $n_e = 10^8\ cm^{-3}$ and electron temperature is set to $T_e = 0.025$ eV. Charged neutrality at the beginning of the pulse is maintained by the addition of the appropriate amount of N_2^+ if necessary.

3. Plasma activation of water

3.1. Base case: multiple-pulse plasma activation of water

Upon application of the 10 kV at the start of each voltage pulse, the small initial electron density, $10^8\ cm^{-3}$, begins to avalanche. Since the impedance of the plasma is large at this time, the voltage across the discharge is essentially the applied voltage, which produces a slowly varying E/N (electric field/gas number density) of $2.0 \times 10^{-15}\ V\ cm^2$ or 200 Td (1 Td $= 10^{-17}\ V\ cm^2$). The electron temperature, T_e, remains at its pre-breakdown value of 4.3 eV until the electron avalanche

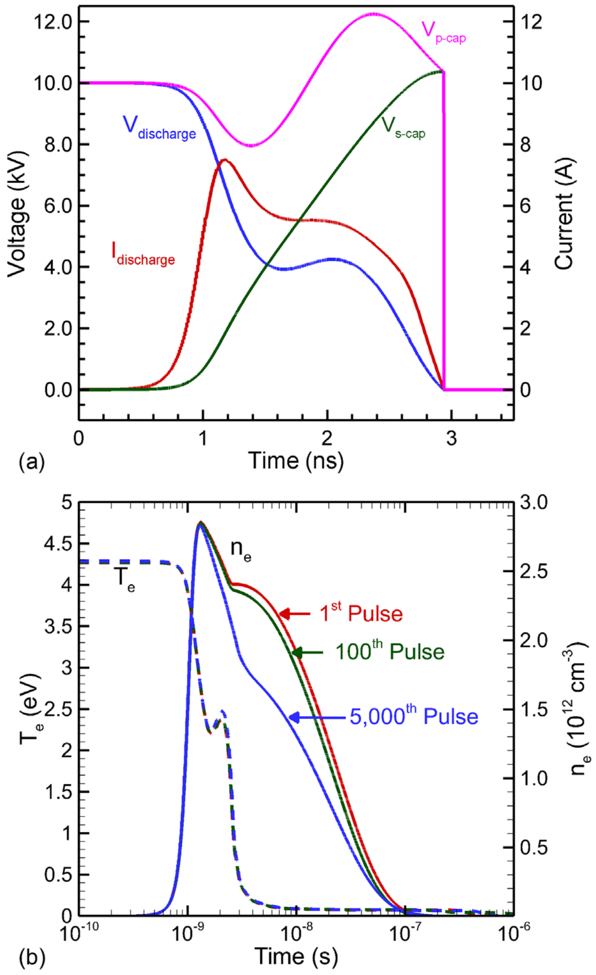

Figure 2. Circuit and plasma parameters during the discharge pulse for the base case. (a) Current and voltage. The combination of the parallel capacitance and inductance produces a local peak in discharge voltage at 2 ns. (b) Electron temperature (T_e) and density (n_e) during the 1st pulse, 100th pulse, and 5000th pulse. T_e and the maximum value of n_e are unchanged after thousands of pulses, but the electron attachment rates increase at later pulses which decreases n_e.

produces a sufficiently large electron density to lower the impedance and the E/N of the discharge. This occurs when $n_e \approx 6 \times 10^{11}$ cm^{-3}, as shown in figure 2(b). With the decrease in impedance and E/N of the plasma, T_e decreases. The avalanche proceeds, increasing the electron density to a maximum of 2.8×10^{12} cm^{-3} as long as T_e remains above 2.8 eV. Below this value, the net ionization coefficient is negative, attachment to O_2 begins to dominate electron losses, and the electron density decreases. As the discharge current increases, the voltage drop across the series resistance becomes significant, and the discharge voltage further decreases. For this particular circuit, the capacitance in parallel with the discharge and the inductance produce a slight ringing in the discharge voltage. T_e follows the discharge voltage closely, and this ringing in discharge voltage is reflected in T_e. Note that at $t = 2.4$ ns and $T_e \approx 2.1$ eV, the rate of electron loss decreases. The attachment to O_2 in atmospheric pressure plasmas has two components—3-body attachment which consumes thermal electrons and 2-body dissociative attachment which has a threshold energy. Over this range of electron temperature, the rate of 2-body attachment decreases as T_e decreases, thereby decreasing the total rate of electron loss. For these conditions, the duration of the current pulse is determined by the charging of the dielectric which is represented by the series capacitance.

As discussed below, with each successive discharge pulse, the composition of the ambient gas changes with the accumulation of products initiated by dissociation of the feedstock gases. The changes in composition of the gas on the basis of mole-fraction are relatively small. After 5000 pulses, species other than the feedstock species (N_2, O_2, H_2O, CO_2) have a mole fraction of only 7.3×10^{-3}. However, even these small changes in composition in the gas at the beginning of a discharge pulse affect the characteristics of the discharge. For example, the electron temperature and electron density are shown in figure 2(b) for the 1st, 100th and 5000th pulse. T_e is not particularly affected by these long timescale changes in composition. The value of T_e is in large part determined by the rate of electron energy loss as a function of T_e and the rate of avalanche which determines the impedance and so the E/N of the discharge. Both of these parameters are dominated by the major constituents of the gas. It is also for this reason that the maximum electron density does not appreciably change with successive pulses.

Electron losses can, however, be significantly affected by species having small mole fractions, particularly for processes that attach low energy or thermal electrons. For our conditions, the accumulation of ozone (O_3) and nitrous oxide (N_2O) on a pulse-to-pulse basis results in more attachment during the afterglow of the discharge pulse which produces a more rapid decrease in electron density. The dissociative attachment processes to O_3 are

$$e + O_3 \rightarrow O_2 + O^-, \tag{8a}$$

$$e + O_3 \rightarrow O_2^- + O, \tag{8b}$$

which have a total rate coefficient of 8×10^{-10} cm^3 s^{-1} when $T_e = 2.9$ eV (corresponding to the maximum power deposition). N_2O, undergoes dissociative attachment,

$$e + N_2O \rightarrow O^- + N_2, \tag{9}$$

with rate coefficient 2×10^{-10} cm^3 s^{-1} when $T_e = 2.9$ eV.

Since the air above the water is humid, the polar gas-phase water molecules often surround the ions in the afterglow forming water-cluster ions, denoted by $M^+(H_2O)_n$ or $M^-(H_2O)_n$ [38, 39]. The initial ions form cluster-ions in tens of ns. The ion–ion plasma containing mostly cluster ions decays several orders of magnitude between pulses, but does not fully recombine before the next pulse. Although the addition of water molecules to water cluster ions is exothermic up to 5–10 water molecules in humid atmospheric pressure environments [40], the reaction mechanism in this study was simplified to having clusters with no more than two water molecules.

Densities of ions which trace their origins to O_2, N_2 and H_2O are shown in figure 3 during the discharge pulse and afterglow for the 1st, 100th and 5000th pulses. For ions which trace their origins to O_2, the dominant positive ion during the

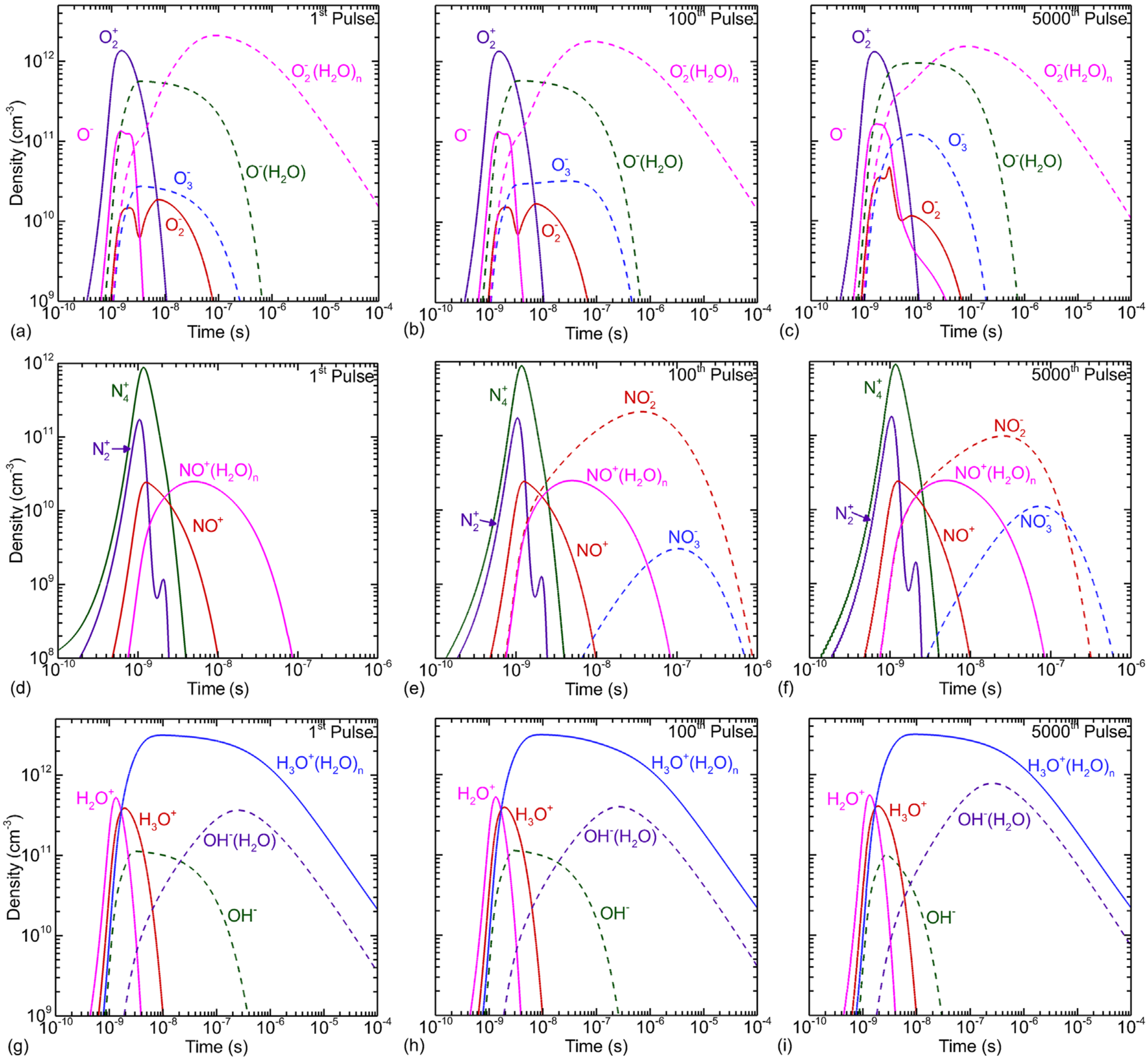

Figure 3. Densities of gas phase charged species during the discharge pulse and afterglow in the base case after the 1st, 100th and 5000th pulses. These species are roughly grouped into those originating from (a)–(c) O_2, (d)–(f) N_2 and (g)–(i) H_2O. The negative ion dynamics evolve over the 5000 pulses due to the accumulation of neutral species, however the positive ion dynamics are less affected. The high humidity in this case results in the formation of water cluster ions.

avalanche phase of the discharge pulse is O_2^+. Formation of O_4^+ follows by 3-body associative charge exchange, though its density is two orders of magnitude lower during the discharge pulse. The O_2^+ and O_4^+ then charge exchange with the ambient H_2O forming H_2O^+. O_2^- forms on two different timescales, producing the bimodal curve shown in figure 3. The first peak is due to charge exchange from O^- to O_2 and occurs while the T_e is still elevated. The formation of O^- is significant only during the discharge pulse since dissociative electron attachment to O_2 has a threshold energy of 3.6 eV. The second peak in O_2^- is due to three body attachment to O_2, which has a maximum at $T_e = 0.06$ eV, so the rate of reaction is largest as T_e is falling. Over several thousand pulses, the first peak in O_2^- density increases because of accumulation of O_3, and the dissociative attachment reactions shown in equation (8). The second peak decreases with increasing pulses since the electron density more rapidly decreases, and there are fewer electrons available when $T_e = 0.06$ eV.

The production of O_3^- has three dominant sources:

$$O^- + O_2 + M \rightarrow O_3^- + M, \tag{10a}$$

$$O^- + O_3 \rightarrow O + O_3^-, \tag{10b}$$

$$O_2^- + O_3 \rightarrow O_2 + O_3^-. \tag{10c}$$

As O_3 accumulates over many pulses, O_2^- and O^- densities increase during the first 10 ns, and as a result the O_3^- production increases as well. The surviving O^- and O_2^- are eventually converted to water cluster ions. At times exceeding hundreds of microseconds, $O^-(H_2O)$ and $O_2^-(H_2O)_n$ are the surviving negative ions.

For ions tracing their origin to nitrogen, N_2^+ is first formed by electron impact ionization of N_2 but quickly undergoes associative charge exchange to form N_4^+, which has the highest density of any nitrogen-containing ion during all discharge pulses. The larger RNS, such as NO_2, NO_3, N_2O_4, HNO_3, take several

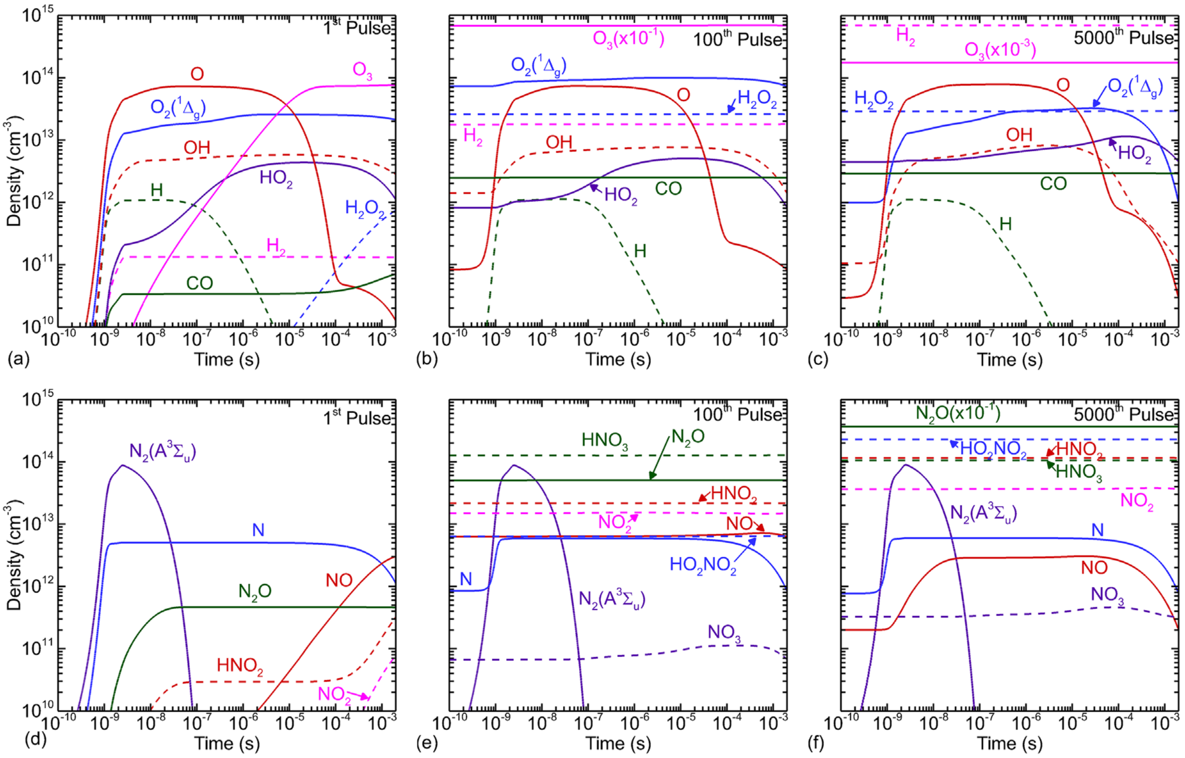

Figure 4. Densities of gas phase neutral species during the discharge and afterglow in the base case after the 1st, 100th and 5000th pulses. These species are grouped into those ((a)–(c)) without nitrogen and ((d)–(f)) those containing nitrogen. Several neutral species accumulate over many pulses, but the more reactive species form and are consumed with each pulse.

reactions to form, are not particularly reactive in the gas phase, and therefore accumulate over many pulses. Nitrite (NO_2^-) has a negligible density on the first pulse and increases to be one of the dominant negative ions with a density of 2×10^{11} cm^{-3} during later pulses. As HNO_3 accumulates from the 1st to 100th pulse, dissociative attachment produces NO_2^-,

$$e + HNO_3 \rightarrow NO_2^- + OH. \tag{11}$$

As O_3 accumulates from the 100th pulse to the 5000th pulse, the charge exchange reaction

$$O_3 + NO_2^- \rightarrow NO_3^- + HNO_2, \tag{12}$$

rapidly converts NO_2^- to nitrate (NO_3^-) and is the primary source of NO_3^-.

The densities of N^+, NO^+, NO_2^+ and $NO^+(H_2O)_n$ are little affected by the accumulation of species over the succession of pulses. These ions indirectly come from electron impact ionization of the N_2 and O_2 followed by

$$O^+ + N_2 + M \rightarrow NO^+ + N + M, \tag{13a}$$

$$N_3^+ + O_2 \rightarrow NO_2^+ + N_2, \tag{13b}$$

where O^+ is produced dominantly by dissociative ionization of O_2 and secondarily by direct ionization of O, though this is a small source. N_3^+ is the result of dissociative ionization of N_2 (or direct ionization of N, though this is also a small source) followed by the reaction $N^+ + N_2 + M \rightarrow N_3^+ + M$. Although direct electron impact of NO, NO_2, and N_2O can produce NO^+ and NO_2^+, their contributions are not significant even after 5000 pulses of accumulation.

H_2O^+ is formed by direct electron impact ionization of H_2O in the gas phase and from charge exchange from N_2^+, N_4^+, and O_2^+ to H_2O. H_2O^+ reaches a density of 6×10^{11} cm^{-3}, but is quickly depleted in formation of hydronium, H_3O^+, by,

$$H_2O + H_2O^+ \rightarrow H_3O^+ + OH, \tag{14a}$$

$$OH + H_2O^+ \rightarrow H_3O^+ + O. \tag{14b}$$

H_3O^+ forms cluster ions, $H_3O^+(H_2O)_n$ which is the cluster ion having the maximum density with each pulse. OH^- and its cluster ion are the most abundant anions originating from H_2O with a maximum density of 7×10^{11} cm^{-3}. The OH^- forms by dissociative attachment ($e + H_2O \rightarrow OH^- + H$) to H_2O. There is some H^- formation by an analogous dissociative attachment process, but its production is limited to the first 2 ns when T_e is high, and so its density is an order of magnitude smaller than OH^-. The lifetime of OH^- decreases with successive discharge pulses as it charge exchanges with the increasing density of O_3 to form with O_3^-, which helps buoy the density of O_3^-. During early pulses when the density of O_3 is low, OH^- is slowly consumed, and so the O_3^- density remains fairly low at 2×10^{10} cm^{-3} until 100 ns at which point the density of OH^- begins to decrease. By the 5000th pulse, OH^- is rapidly consumed by charge exchange to O_3, producing a density of O_3^- in excess of 10^{11} cm^{-3}. Depletion of OH^- also occurs through formation of $OH^-(H_2O)_n$, however the density of this cluster ion also increases with the accumulation of O_3. The density of $O^-(H_2O)_n$ increases with O_3, which in turn generates $OH^-(H_2O)_n$ in the reaction $O^-(H_2O)_n + H_2O \rightarrow OH^-(H_2O)_n + OH$. In this way the buildup of O_3 depletes OH^-, but increases the density of $OH^-(H_2O)_n$.

From this analysis, we find that stable neutral products accumulate over thousands of pulses in humid air plasmas, which in turn affect the density and identity of anions. For these particular conditions, much of this multi-pulse anion chemistry can be traced to the accumulation of O_3. Therefore increases in gas temperature, which typically reduce the accumulation of O_3, would have a second order effect on the anion densities. The gas phase cations produced at each pulse are less affected by the accumulation of neutrals due, in large part, to the high humidity. The formation of H_3O^+ and its clustering with water represents the terminal cation, a process that is little affected by the accumulation of reactant products.

The densities of ROS and RNS are shown in figure 4 during the 1st, 100th and 5000th pulses. These species can be divided into three categories based on the timescales of their evolution. During each discharge pulse, short-lived species are formed by electron impact and are generally quenched or consumed by reactions prior to the next pulse. $N_2(v)$, $O_2(v)$, $N_2(A^3\Sigma_u)$, and $O_2(^1\Sigma_u)$ are in this group. A second set of species achieve a quasi-steady state density which modulates on a pulse-to-pulse basis as the species is produced and consumed. These species include O, OH, HO_2, $O_2(^1\Delta_g)$, N, NO, and NO_3. Finally, the third set of species have long lifetimes with densities that accumulate from pulse-to-pulse. These species either continue to accumulate through the last pulse or reach a steady state density. In either case, the timescales of the dynamics are much longer than the interpulse period of 2 ms. O_3, H_2O_2, CO, N_2O, HNO_2, NO_2, and HNO_3 are in this category.

A large fraction of the power deposition is expended in forming the vibrational and electronic excited states of N_2 and O_2. The vibrationally excited states $O_2(v)$ and $N_2(v)$ are generated with densities up to 6×10^{14} cm^{-3} and 2×10^{13} cm^{-3}. This stored energy contributes to gas heating by vibrational-translational (V-T) collisions on microsecond timescales. The first metastable electronically excited state of N_2, $N_2(A^3\Sigma_u)$, is rapidly quenched by O_2 through dissociative excitation and excitation transfer [41]. $O_2(^1\Sigma_u)$, the second excited state of O_2, is rapidly quenched by collisions with water vapor to form $O_2(^1\Delta_g)$. The production of electronically excited states also affects the discharge by two-step electron impact ionization and dissociation processes, which can enable more ionization at a lower T_e. Electron impact dissociation of H_2O produces H, which reacts to form H_2 ($H + H + M \rightarrow H_2 + M$) in a few microseconds, so H does not accumulate.

In the second set of species, the only electronic excited state that lasts beyond a few microseconds is $O_2(^1\Delta_g)$, with a collisional lifetime on the order of the interpulse period (2 ms). As a result, there is some accumulation of $O_2(^1\Delta_g)$ on a pulse-to-pulse basis. Most of the O atoms, produced by electron impact dissociation of O_2 and dissociative quenching of $N_2(A^3\Sigma_u)$ by O_2, are consumed in making ozone, $O + O_2 + M \rightarrow O_3 + M$, and this is the primary source of O_3. This reaction occurs within 100 μs and so O is mostly depleted with each pulse.

Electron impact dissociation of H_2O produces OH which combines to form H_2O_2 ($OH + OH + M \rightarrow H_2O_2 + M$), and the H_2O_2 accumulates to a density of 3×10^{13} cm^{-3}. This conversion takes slightly longer than the interpulse period of 2 ms, so there is some accumulation of OH from pulse to pulse. HO_2 is mainly produced by $H + O_2 + M \rightarrow HO_2 + M$, but there are other reactions which contribute to its production. HO_2 is produced in hundreds of nanoseconds to several microseconds after the pulse, rather than during the discharge pulse as do species which result directly from electron impact processes. HO_2 is dominantly consumed by,

$$OH + HO_2 \rightarrow H_2O + O_2, \tag{15a}$$

$$HO_2 + O_2(^1\Delta_g) \rightarrow OH + O_2 + O. \tag{15b}$$

Nitrogen atoms produced by electron impact dissociation of N_2 are not a highly reactive species on their own at ambient temperatures, and so a large fraction of N atoms simply recombine to form N_2. However, their presence contributes significantly to formation of N_xO_y (especially NO) and HNO_x through reactions with ROS. NO primarily forms by $O_2 + N \rightarrow NO + O$ during early pulses. However, during later pulses N_2O begins to accumulate, and the reaction $N_2(A^3\Sigma_u) + N_2O \rightarrow N_2 + N + NO$ dominates the formation of NO. As a result, during later pulses, NO forms dominantly during the discharge pulse when the density of $N_2(A^3\Sigma_u)$ is large, instead of during the afterglow. NO_2 and NO_3 are intermediate species to the formation of acids, and can also form higher order RNS (N_2O_3, N_2O_4, N_2O_5) which further facilitate acid formation.

The densities of the reactive species O, NO, $O_2(^1\Delta_g)$ and OH at the end of each interpulse period have a counter intuitive evolution over long time scales. These are species that undergo transients during each pulse—generation followed by consumption, but are not completely depleted before the next pulse. The consumption following each pulse increases with pulse number, resulting in their decaying to lower densities between pulses at the 5000th pulse compared, for example, to the 100th pulse. Although their production during each pulse changes very little, the consumption of these species is more rapid as the gas phase RONS accumulate. These consuming reactions include

$$O + O_3 \rightarrow O_2 + O_2, \tag{16a}$$

$$O + NO_2 + M \rightarrow NO_3 + M, \tag{16b}$$

$$NO + O_3 \rightarrow NO_2 + O_2, \tag{16c}$$

$$O_2(^1\Delta_g) + O_3 \rightarrow O_2 + O_2 + O, \tag{16d}$$

$$OH + O_3 \rightarrow HO_2 + O_2. \tag{16e}$$

The presence of O_3 produces some additional O by dissociative attachment forming O_2^-, however in later pulses accumulating O_3 reacts with any remaining O.

The third group of species, with reactive timescales much longer than the interpulse period (here, 2 ms), includes several relatively stable species: H_2O_2 (from $OH + OH + M \rightarrow H_2O_2 + M$), O_3 (from $O + O_2 + M \rightarrow O_3 + M$), N_2O (from $O_2 + N_2(A^3\Sigma_u) \rightarrow N_2O + O$), and HNO_3. These species are generally unreactive in the absence of organic molecules and at ambient temperatures. Most of these stable species react with other reactive species (e.g. N_2^+, O), but not with other accumulated neutrals. Other species in this category are reactive, but have longer reactive timescales. The cluster species HO_2NO_2 forms by $HO_2 + NO_2 + M \rightarrow HO_2NO_2 + M$, is stable in air and accumulates to 2×10^{14} cm^{-3}. NO_2 has long timescale dynamics, and is slowly converted to HNO_3 by $NO_2 + OH + M \rightarrow HNO_3 + M$. This reaction limits its maximum density to 1×10^{14} cm^{-3}. HNO_2 is a weak acid which accumulates to a density of 1×10^{14} cm^{-3} over many pulses, and eventually forms HNO_3.

During the long timescales (seconds to 10 s) diffusion losses by solvation to the liquid can be significant for this group of species. The fraction of the gas phase density that can be transferred from the gas to the liquid is a function of the Henry's law equilibrium constant. Species whose densities continue to increase through the 5000th pulse include H_2, O_3, N_2O, HNO_2, HO_2NO_2, and NO_2, all of which have lower Henry's law constants and, therefore, lower rates of loss by solvation into the liquid. Species with the highest Henry's law constants, H_2O_2 and HNO_3 reach a steady state because they are lost to the liquid through solvation at the same rate as their production.

3.2. Base case: plasma activated liquid chemistry

During each discharge pulse, fluxes of ions and electrons reach the surface of the liquid as a consequence of ambipolar diffusion. Upon entering the liquid, most of the positive ions (N_2^+, N_4^+, O_2^+, O_4^+, NO^+, H_2^+, NO_2^+ and their corresponding water cluster species) quickly charge exchange with H_2O_{aq}, forming $H_2O^+_{aq}$. The H_2O^+ quickly forms hydronium, $H_3O^+_{aq}$ by reacting with water, $H_2O_{aq} + H_2O^+_{aq} \rightarrow H_3O^+_{aq} + OH_{aq}$. The increasing density of $H_3O^+_{aq}$ then decreases the pH of the water. Electrons quickly solvate, which in our mechanism is represented by $H_2O^-_{aq}$, which then forms O^-_{2aq} by $H_2O^-_{aq} + O_{2aq} \rightarrow H_2O_{aq} + O^-_{2aq}$. Excited state species from the gas phase which enter the water and which have enough energy to dissociate water are assumed to quickly undergo dissociative excitation transfer, $M^*_{aq} + H_2O_{aq} \rightarrow M_{aq} + H_{aq} + OH_{aq}$. The excited state and ion chemistry occurs primarily during the first 100 ns after each pulse. In a spatially resolved model, the majority of these reactions would occur in the near-surface layer. Almost all of the rest of the neutral chemistry in the liquid happens over timescales longer than the interpulse period of 2 ms, accumulating over several pulses, as shown in figure 5. In a spatially resolved model, these reactions would occur deeper in the liquid.

Several acids formed in the gas or liquid dissociate in the liquid, generating $H_3O^+_{aq}$, and lowering the pH of the water. Nitric acid (HNO_{3aq}) is a strong acid which dissociates to form NO^-_{3aq}, and it is the largest contributor to the plasma-induced acidification of the liquid. This acidification results in an $H_3O^+_{aq}$ density of 5×10^{16} cm^{-3} (8×10^{-5} M), and a final pH of 4.1 at the end of 5 min. For weak acids, which only partially dissociate, this process is described by pK_a, where

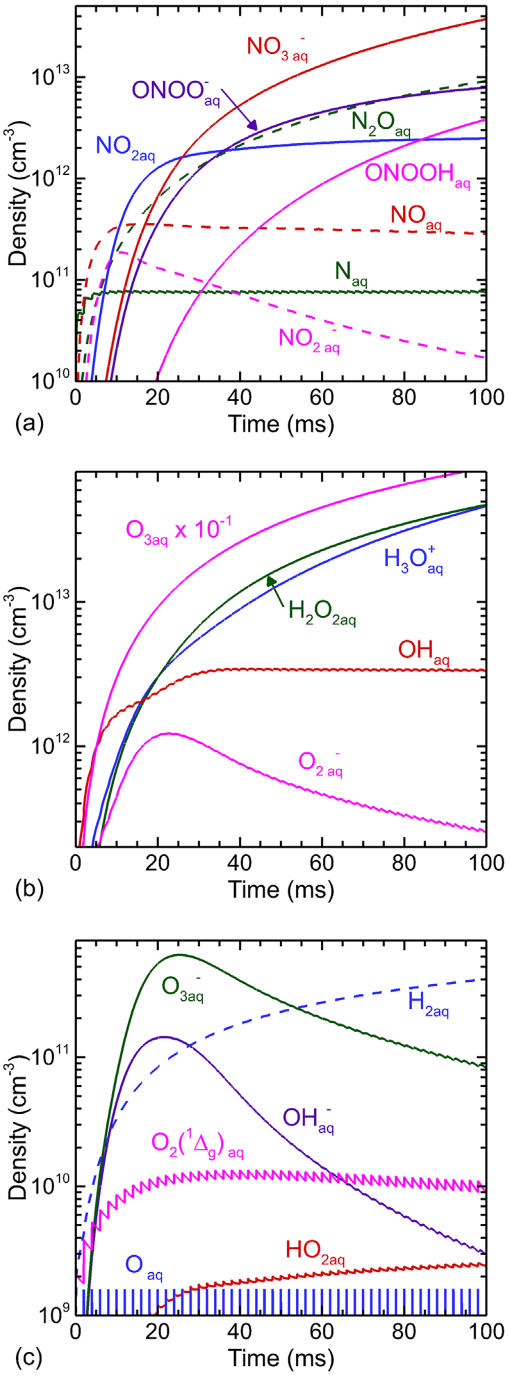

Figure 5. The densities of aqueous (a) RNS and (b) and (c) ROS for the first 50 pulses of the base case. The most reactive species, including many ions and excited states were omitted as they appear as delta functions on these timescales. Several species establish a pulsed equilibrium, while the others evolve over timescales much longer than the interpulse period. A concentration of 1 M is equivalent to a number density 6×10^{20} cm^{-3}.

$pK_a = -\log(K_a)$. K_a is the acid dissociation constant which is the equilibrium value of the products of the conjugate ions to the acid. In our reaction mechanism, these processes are represented by two reactions for each acid

$$HA_{aq} + H_2O_{aq} \rightarrow H_3O^+_{aq} + A^-_{aq}, \qquad (17a)$$

$$H_3O^+_{aq} + A^-_{aq} \rightarrow HA_{aq} + H_2O_{aq}. \quad (17b)$$

The ratio of the reactions rates is 10^{-pK_a}. (The liquid in this study does not contain a pH buffer.) Weak acids produced by the plasma include HNO_{2aq} ($pK_a = 3.4$), HO_{2aq} ($pK_a = 4.8$) and $ONOOH_{aq}$ ($pK_a = 6.8$). pK_a is the approximate value of the pH above which the weak acid will be mostly in dissociated form (A^-_{aq}). So HNO_{2aq} will be mostly in the form NO^-_{2aq} even as the liquid pH drops to 4.1. However, $ONOO^-_{aq}$ will revert back to $ONOOH_{aq}$ once the pH falls below 6.8.

O_{3aq} is a dominant ROS in the liquid accumulating to 5×10^{16} cm^{-3} (8×10^{-5} M), primarily from the solvation of gas phase O_3. The negative ion O^-_{3aq} then forms by $O^-_{2aq} + O_{3aq} \rightarrow O_{2aq} + O^-_{3aq}$. $O_2(^1\Delta_g)$ solvates from the gas resulting in 1×10^{10} cm^{-3} (2×10^{-11} M) of $O_2(^1\Delta_g)_{aq}$, which decays by excitation transfer to H_2O_{aq}.

OH_{aq} has several significant sources including the solvation of gas phase OH and $O_{aq} + H_2O_{aq} \rightarrow OH_{aq} + OH_{aq}$. OH_{aq} rapidly forms H_2O_{2aq}. HO_{2aq} comes from solvation of HO_2 as well as from $O_{2aq} + H_{aq} \rightarrow HO_{2aq}$.

In general, in spite of there being a small equilibrium density of N_{2aq} in the liquid, the source of aqueous RNS is dominantly from N_xO_y species generated in the gas phase solvating into the liquid. The dominant reactions of N_xO_{yaq} are formation of acids, HNO_{xaq}. For example,

$$NO_{2aq} + NO_{2aq} + H_2O_{aq} \rightarrow HNO_{3aq} + HNO_{2aq}, \quad (18a)$$

$$NO_{aq} + NO_{2aq} + H_2O_{aq} \rightarrow HNO_{2aq} + HNO_{2aq}, \quad (18b)$$

$$NO_{2aq} + H_{aq} \rightarrow HNO_{2aq}, \quad (18c)$$

$$NO_{2aq} + OH_{aq} \rightarrow HNO_{3aq}, \quad (18d)$$

$$N_2O_{4aq} + H_2O_{aq} \rightarrow HNO_{3aq} + HNO_{2aq}, \quad (18e)$$

$$N_2O_{5aq} + H_2O_{aq} \rightarrow ONOOH_{aq} + ONOOH_{aq}. \quad (18f)$$

These acids can then dissociate by hydrolysis,

$$HNO_{3aq} + H_2O_{aq} \rightarrow NO^-_{3aq} + H_3O^+_{aq} \quad (19a)$$

$$HNO_{2aq} + H_2O_{aq} \rightarrow NO^-_{2aq} + H_3O^+_{aq} \quad (19b)$$

$$ONOOH_{aq} + H_2O_{aq} \rightarrow ONOO^-_{aq} + H_3O^+_{aq}. \quad (19c)$$

As a result of these reactions, NO^-_{3aq} continues to accumulate in the liquid through the 5000th pulse with a density of 5×10^{16} cm^{-3} (8×10^{-5} M). Peroxynitrous acid ($ONOOH_{aq}$) primarily forms by the reaction equation (18*f*). Because peroxynitrous acid ($ONOOH_{aq}$) and its conjugate base, peroxynitrite ($ONOO^-_{aq}$), undergo different reactions, its lifetime and chemistry depends on pH. $ONOOH_{aq}$ isomerizes to form HNO_{3aq} or dissociates into OH_{aq} and NO_{2aq} in hundreds of ms. It is more stable in its dissociated form, peroxynitrite ($ONOO^-_{aq}$).

The cluster species HO_2NO_{4aq}, solvated from the gas phase, thermally decays to HO_{2aq} and NO_{2aq} with a time constant of several seconds, providing a mechanism to deliver radicals over much longer timescales than the application of plasma to the liquid. This reaction becomes important during the afterglow in the liquid. N_2O is a stable species in both the gas and liquid, originates with gas phase reactions and solvates to densities of 4×10^{15} cm^{-3} (7×10^{-6} M) in the liquid.

In plasma–liquid systems that have quiescent liquids, the top layer of the liquid can become saturated at their Henry's law equilibration value by in-diffusing gas phase species. At that point, the in-coming diffusion terminates until the aqueous species either diffuse from the surface to reduce the density at the surface below their equilibrium value, or their densities decrease by reactions. In a system with a convectively dominated liquid, the in-coming solvated species are well-mixed in the entire liquid, which then reduces their densities near the surface and allows in-coming diffusion to continue. On very long time scales in *a non-reactive system*, the final densities for both systems will eventually reach the equilibrium value in the entire liquid volume. However, on intermediate times scales (short compared to in-liquid diffusion times but long compared to convective times) the well-stirred liquid is able to accept a larger fluence of reactants from the gas phase than a system that is not well-stirred. The well-stirred assumption used here should be considered an upper limit of the ability of the liquid to accept reactivity from the gas phase. The lack of a saturated liquid layer makes the solvation kinetics less sensitive to limitations on accepting reactants from the gas phase determined by Henry's law constants.

3.3. Base case: afterglow chemistry

After 5000 discharge pulses lasting 10 s, power is removed from the DBD, and the system continues to evolve during the afterglow. Ions in the gas recombine in hundreds of microseconds after the plasma pulse, so they do not continue to deliver reactivity to the liquid during the afterglow. In the absence of gas flow, the reactive neutrals remain in the gas above the liquid until they are consumed by reactions or solvate into the liquid. First, we will discuss the behavior of the gas phase reactive neutrals.

The densities of gas phase species up to 5 min into the afterglow are shown in figure 6. Two distinct phases of decay occur for H_2O_2, HO_2NO_2, N_2O_5, HNO_3, HNO_2 and NO_2. For approximately 1 s after the discharge pulses terminate, the loss of these species is dominated by diffusion and solvation into the liquid while there are also small rates of production. After 1 s, the densities drop low enough that the rates of diffusion loss are on the order of their production rates. It is also possible that the diffusion into the liquid would slow when the density in the liquid approaches its equilibrium value given by Henry's law. However, that is not the case here. O_3 and N_2O do not follow this pattern because the ratio of their densities in the gas and the liquid are already close to their Henry's law equilibrium values due to their low Henry's law constant. The most reactive species, [OH, O, $O_2(^1\Delta_g)$, HO_2, N, NO] have gas-phase reaction rates with timescales much shorter than diffusion and so their losses are dominated by gas phase kinetics.

The densities of aqueous species are shown in figure 7 during the afterglow. In the liquid, the change in densities of most species results from reactions as opposed to transport. Diffusion out of the liquid into the gas can occur if a species

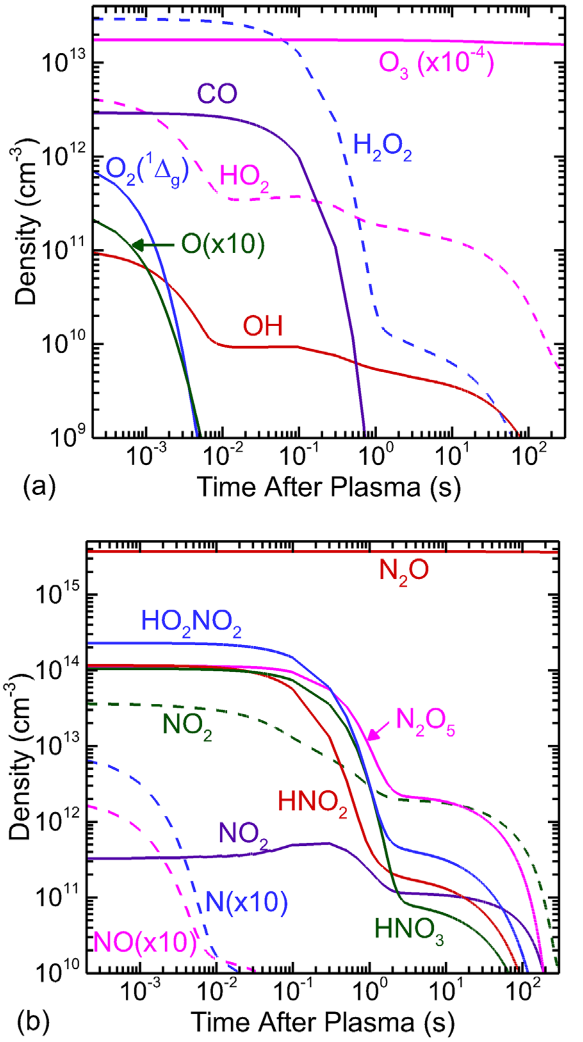

Figure 6. Afterglow evolution of densities of gas phase (a) ROS and (b) RNS. The time is relative to the end of the last discharge pulse. The species densities decrease due to solvation into the liquid during seconds of afterglow.

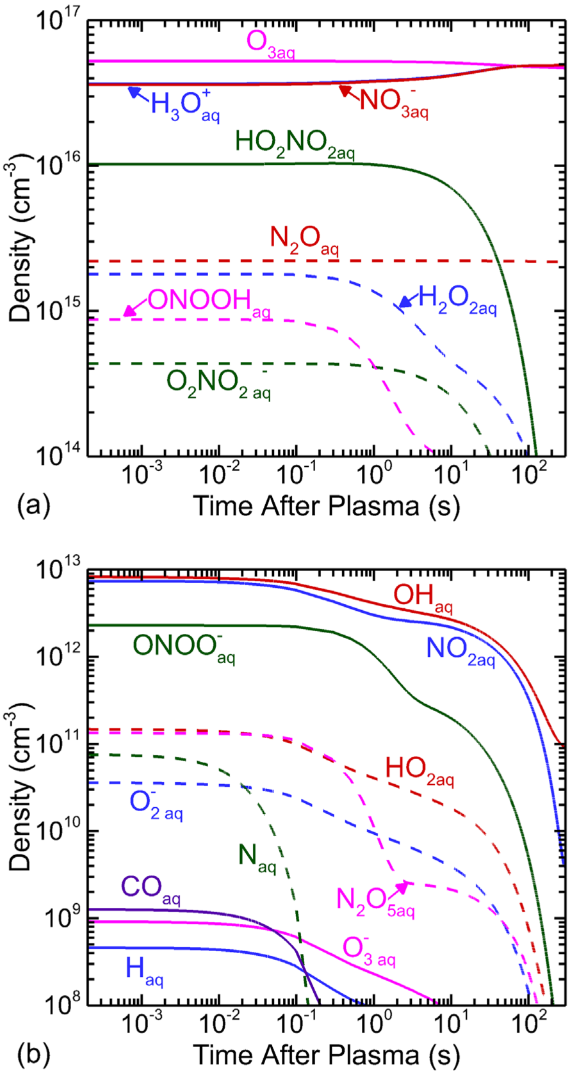

Figure 7. The decay of reactivity in liquid after the treatment has been completed for species with densities (a) above 10^{14} cm^{-3} and (b) below 10^{13} cm^{-3}. Time is relative to the end of the last pulse. Gas phase RONS continue to solvate during the afterglow, which provides a source of these liquid resident RONS. Reactions deplete most of the RONS at long timescales.

is over-saturated, but it is not significant in this system. The most prevalent plasma produced species in the liquid are O_{3aq} and NO^-_{3aq}. The cluster species HO_2NO_{2aq} thermally decays to HO_{2aq} and NO_{2aq} with a time constant of several seconds. The resulting NO_{2aq} reacts with H_2O_{aq} to form HNO_{2aq} or HNO_{3aq}, which accounts for the increase in NO^-_{3aq} on timescales of tens of seconds. The HO_{2aq} hydrolyzes to form $H_3O^+_{aq}$ and O^-_{2aq}. HO_{2aq} also reacts with OH_{aq} to form O_{2aq} and H_2O. Although H_2O_{2aq} is stable in pure water at room temperature, in this system the reaction $OH_{aq} + H_2O_{2aq} \rightarrow H_2O_{aq} + O^-_{2aq}$ results in its consumption.

$ONOOH_{aq}$ isomerizes to form HNO_{3aq} or breaks down into OH_{aq} and NO_{2aq} in hundreds of ms, so it is more stable in its hydrolyzed form, $ONOO^-_{aq}$. This provides a source of OH_{aq} on long timescales.

3.4. Applied voltage

Parametric studies were performed for otherwise identical conditions to the base case while varying the applied voltage, from 8 kV to 14 kV. It is expected that most species should increase in density with increasing voltage, due to the higher energy deposition. In this case, the total energy deposition over 5000 pulses varies from 0.8 J cm^{-3} (8 kV) to 1.6 J cm^{-3} (14 kV). The maximum electron density increases from 9×10^{11} cm^{-3} (8 kV) to 1.2×10^{13} cm^{-3} (14 kV), and T_e varies from 3.7 eV to 5.5 eV. The peak gas temperature in all cases does not exceed 303 K. The temperature is kept low primarily as a result of thermal conduction, the last term in equation (3), due to the small diffusion length of the gap. This is a result of the assumption that the surfaces in contact with the plasma are held at 300 K, and a 3 K temperature difference in a 2 mm gap is enough to drive an energy fluence to the walls of 1.6 J cm^{-3} in 10 s. In reality, the gas heating may be higher, depending on the thermal properties of materials in contact with the plasma. In a global model, the energy deposition is averaged over the volume of the reactor, whereas a

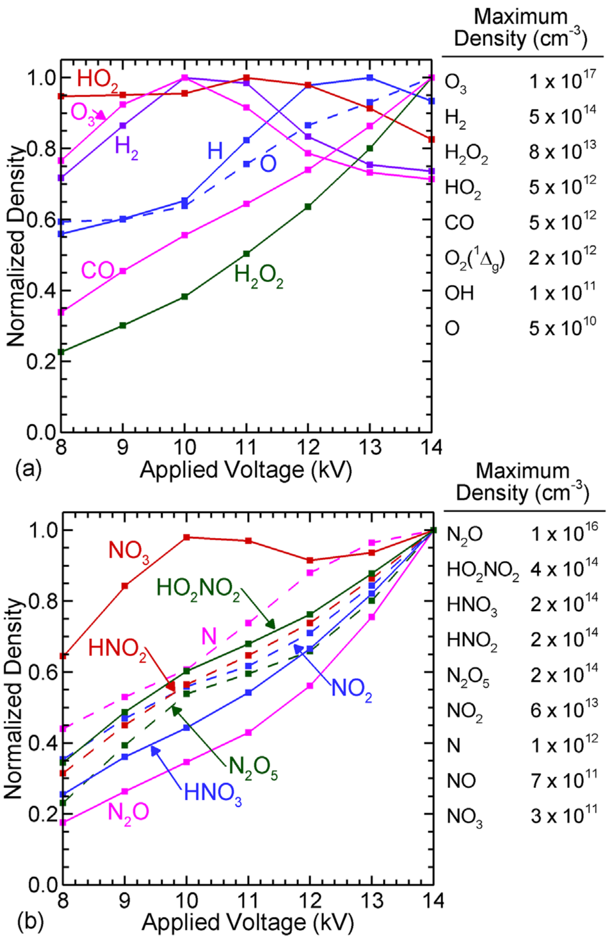

Figure 8. The densities of gas phase (a) ROS and (b) RNS at the end of the last pulse (10 s) for different applied voltages. Values are shown normalized by their maximum density as a function of voltage, shown to the right of each figure. Energy deposition increases with applied voltage, so the density of RONS generally increases.

multi-dimensional model enables energy to be deposited in the smaller volume of the streamer. This latter process can produce locally higher gas temperatures.

The normalized densities of gas phase species as a function of voltage are shown in figure 8 and of aqueous phase species in figure 10. Normalized values are the densities after 5000 pulses (10 s) divided by the maximum value over the parameterized range. The intent here is to show the sensitivity of each species to the independent variable. The normalized densities of gas and liquid RONS after 2 min are shown in figures 9 and 11.

The normalized densities of most species increase approximately linearly with voltage over the range of 8 kV–14 kV. This corresponds to a nearly linear increase of the energy deposition with voltage, which means that the storage capacitor does not fully discharge. The gas phase species following this trend include CO, H_2O_2, O, N, HNO_3, NO_2, N_2O_5, HNO_2, NO_2, N_2O, and HO_2NO_2.

The electron impact dissociation of H_2 ($e + H_2 \rightarrow e + H + H$) has a threshold energy of 8.8 eV, so the rate of this process increases significantly with T_e, and therefore with voltage. This increase in the production of H enables the reaction $H + O_2 + M \rightarrow HO_2 + M$ to produce more HO_2, so a higher voltage favors HO_2 production.

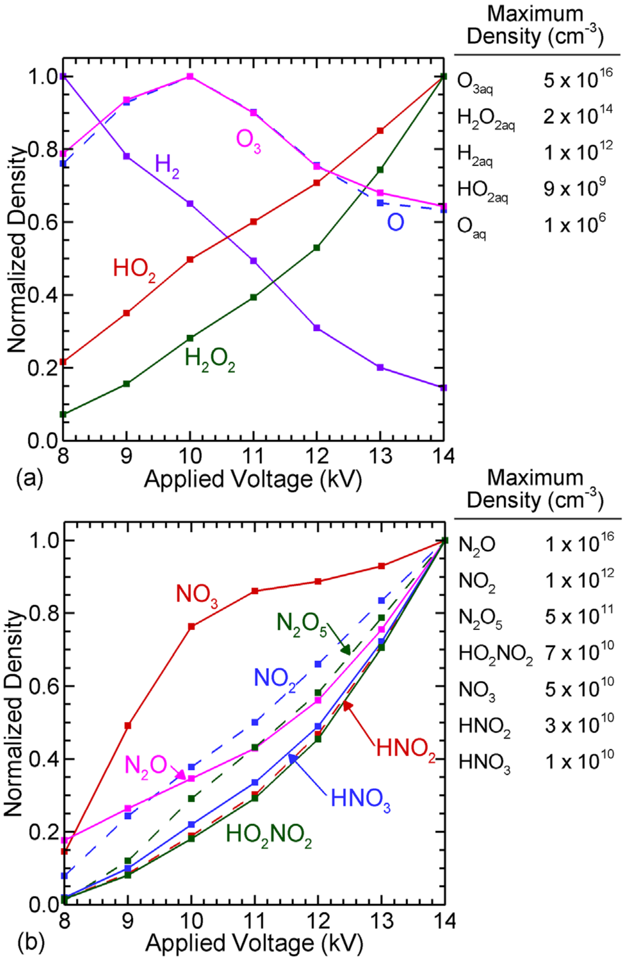

Figure 9. The densities of gas phase plasma produced reactive species at 2 min (10 s treatment and 110 s afterglow) for different applied voltages. (a) ROS and (b) RNS. Values are shown normalized by their maximum density as a function of voltage, shown to the right of each figure. By this time, several of the species (H, O, CO, and N) have decayed to negligible densities.

After 5000 pulses (10 s), the densities of O_3 and H_2 both peak at 10 kV, as shown in figure 8(a). From 8 to 10 kV the inventory of O atoms produced during each pulse increases, leading to production of more O_3 by $O + O_2 + M \rightarrow O_3 + M$. As the voltage continues to rise, the production of O remains relatively constant, however less O ends up in the form of O_3. The density of NO_2 also increases with voltage and consumes much of the O during production of NO_3 (equation (16*b*)). The HO_2 densities at the end of the last pulse are nearly independent of voltage. More HO_2 is produced with higher energy deposition, but more NO_2 is also produced, forming more of the cluster species HO_2NO_2.

Late into the afterglow, (2 min after the start of treatment corresponding to 10 s of plasma treatment followed by 110 s afterglow), species such as H, CO, and N in the gas phase have reacted, and their densities are negligible. The densities of the remaining RONS are shown in figure 9. The density of O is very low at this point, on the order of 10^6 cm^{-3}, but the fact that O_3 can continue to generate O in small amounts at long timescales may be significant in some applications. H_2O_2, O_3, and most of the RNS have the same dependence on voltage as

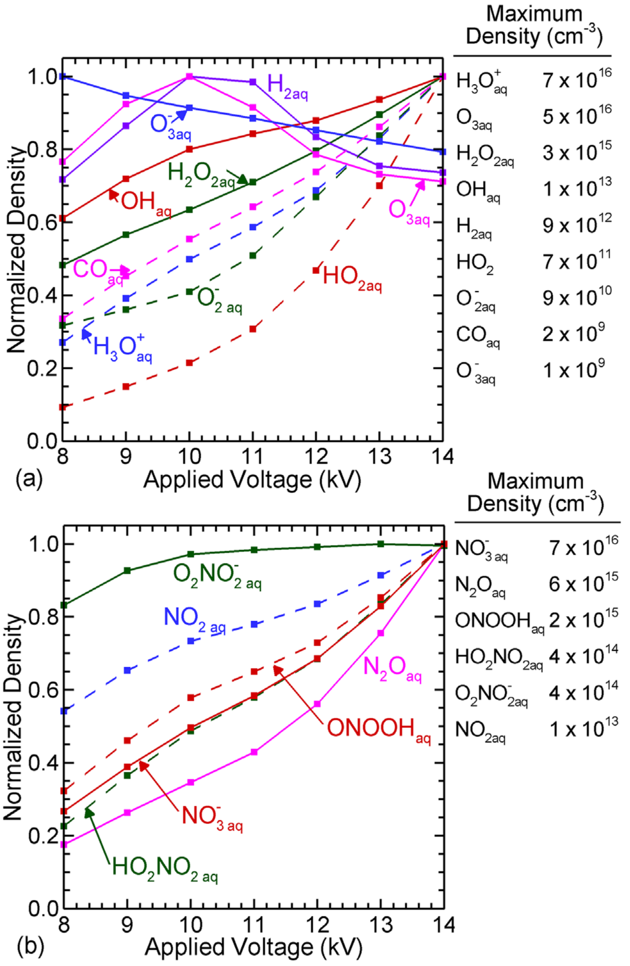

Figure 10. The densities of aqueous plasma produced reactive species at the end of the last pulse (10 s) for different applied voltages. Values are shown normalized by their maximum density as a function of voltage, shown to the right of each figure. (a) ROS and (b) RNS generally increase with voltage, but ROS have a more complex dependence on voltage, making selectivity possible.

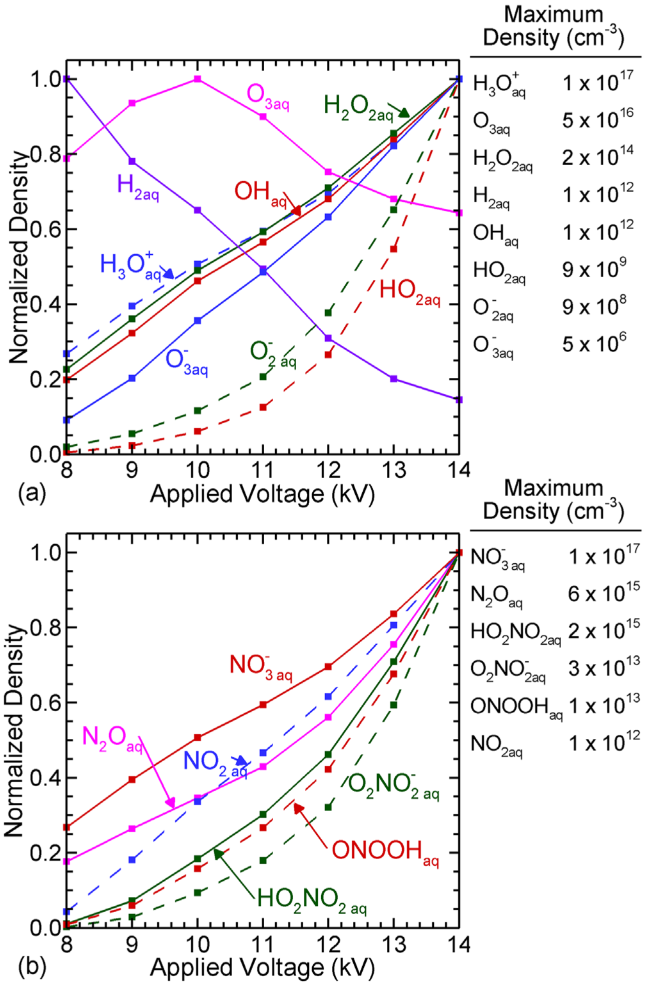

Figure 11. The densities of aqueous plasma produced (a) ROS and (b) RNS for different applied voltages at 2 min (10 s treatment and 110 s afterglow). Values are shown normalized by their maximum density as a function of voltage, shown to the right of each figure.

at the end of the last discharge pulse. The density of H_2 has changed from increasing with voltage after the last discharge pulse (figure 8(a)) to decreasing approximately linearly with voltage after 2 min (figure 9(a)). This change is due to reactions with the liquid, and occurs on long timescales because only a small fraction of the H_2 is solvated at any given time. Although the lifetime of HO_2 in this system is short (in the afterglow, it is consumed by reactions $HO_2 + NO_2 + M \rightarrow HNO_2 + O_2 + M$), it is produced on long timescales by the thermal decay of the cluster HO_2NO_2. At higher voltages, the density of HO_2 remains higher long into the afterglow, as more HO_2 has been stored in HO_2NO_2. This storage of HO_2 results in its density being nearly independent of voltage at 10 s, but increasing with voltage after 2 min. For the RNS, the dependence of the density of NO_3 on voltage changes slightly over 2 min. At higher voltages, there is more NO_2, which can slowly convert to NO_3 long into the afterglow.

The liquid phase species whose densities scale with the energy deposition after 5000 pulses (10 s) are OH_{aq}, H_2O_{2aq}, CO_{aq}, $H_3O^+_{aq}$, NO^-_{3aq}, $ONOOH_{aq}$, N_2O_{aq}, HO_2NO_{2aq} and NO_{2aq}. These densities are shown in figure 10. The voltage dependence of the densities of O_{3aq} and H_{2aq} at the end of the last pulse matches the voltage dependence of their gas phase counterparts (figure 8(a)). This indicates that the production of these species originates predominantly in the gas followed by solvation into the liquid. The density of O^-_{3aq} decreases with applied voltage because it is consumed by $OH_{aq} + O^-_{3aq} \rightarrow HO_{2aq} + O^-_{2aq}$, and at higher voltages, the density of OH_{aq} is larger. The conjugate base of HO_{2aq} is O^-_{2aq}. At lower voltages, the density of O^-_{2aq} is significant, as the pH is close to the pK_a of HO_{2aq}. At higher voltages, the pH is less than the pK_a value, and HO_{2aq} does not dissociate. For the RNS, the conjugate base of HO_2NO_{2aq} is $O_2NO^-_{2aq}$ whose density does not significantly increase for voltages above 10 kV as the liquid becomes too acidic for net dissociation.

After 2 min, the voltage dependence of the densities of OH_{aq}, H_{2aq}, O^-_{3aq}, and $O_2NO^-_{2aq}$ have significantly changed while the voltage dependence of densities of O^-_{2aq}, NO_{2aq}, $ONOOH_{aq}$ and HO_2NO_{2aq} have changed to a lesser extent, as shown in figure 11. OH_{aq} has a short lifetime, so by 2 min, the majority of OH_{aq} that was produced during the plasma-on period has reacted to form H_2O_{2aq}. The OH_{aq} after 2 min arises from a few slow processes, primarily the reaction

$$H_{2aq} + H_2O_{2aq} \rightarrow H_{aq} + OH_{aq} + H_2O_{aq}. \qquad (20)$$

The density of O^-_{3aq} increases with voltage due to its production by charge exchange between O^-_{2aq} and O_{3aq}, both of whose densities increase with voltage. At 10 s, the trend in the density of O^-_{3aq} with voltage is dominated by the reaction $OH_{aq} + O^-_{3aq} \rightarrow HO_{2aq} + O^-_{2aq}$. However, after 2 min, the density of OH_{aq} is too low to significantly affect the density of O^-_{3aq}.

In the afterglow, H_{2aq} is consumed by reaction with H_2O_{2aq} (equation (20)). H_2 has a low Henry's law constant, so most of the H_2 resides in the gas. However, H_2O_2 has a large Henry's law constant, so most of the H_2O_2 resides in the liquid. This means that the reaction between these two species is limited by the transport of H_2 from the gas to the liquid. Since the density of H_2O_{2aq} increases with energy deposition, after a long enough afterglow, H_2 and H_{2aq} both decrease with increasing voltage.

O^-_{2aq} and $O_2NO^-_{2aq}$ are both the dissociated forms of weak acids with a $pK_a = 4.8$. During the afterglow, the pH continues to decrease due to transport of RNS from the gas phase and acid formation. At low voltage, these changes in pH are more significant and have a larger influence on the fractional dissociation of these weak acids. As a result, from 10 s to 2 min, both species have a relative decrease in density at low voltage.

The densities of NO_{2aq}, HO_{2aq}, $ONOOH_{aq}$, and HO_2NO_{2aq} are more sensitive to voltage at 2 min than at 10 s. The densities of these species fall more rapidly at low voltages. There is less stored HO_2NO_{2aq} at low voltage, so it is depleted more rapidly in the liquid. NO_{2aq} and HO_{2aq} production at long timescales is a result of the slow decay of HO_2NO_{2aq}, so they follow the same dependence as HO_2NO_{2aq}. $ONOOH_{aq}$ production at long timescales is an indirect result of this slow decay by the reaction $NO_{aq} + HO_{2aq} \rightarrow ONOOH_{aq}$.

3.5. Gas flow rate

In most experiments using DBDs to treat liquids and tissue, there is no deliberate effort to control the flow of gas through the volume in which the plasma is sustained. Some mixing of the gas in the plasma region with the ambient gas is expected from natural convection. On the other hand, forced convection could be used as a control mechanism for regulating RONS in both the gas and liquid phases. To investigate these possibilities, forced convective flow was included in the model. The resulting normalized densities of gas phase species are shown in figure 12 and of aqueous phase species in figure 13 after 5000 pulses. Important scaling parameters in varying the flow rate are the residence time of the gas in the discharge region (τ_r) and the interpulse period (τ_p). Their ratio, τ_r/τ_p is the average number of discharge pulses each gas molecule is exposed to before it flows out of the system.

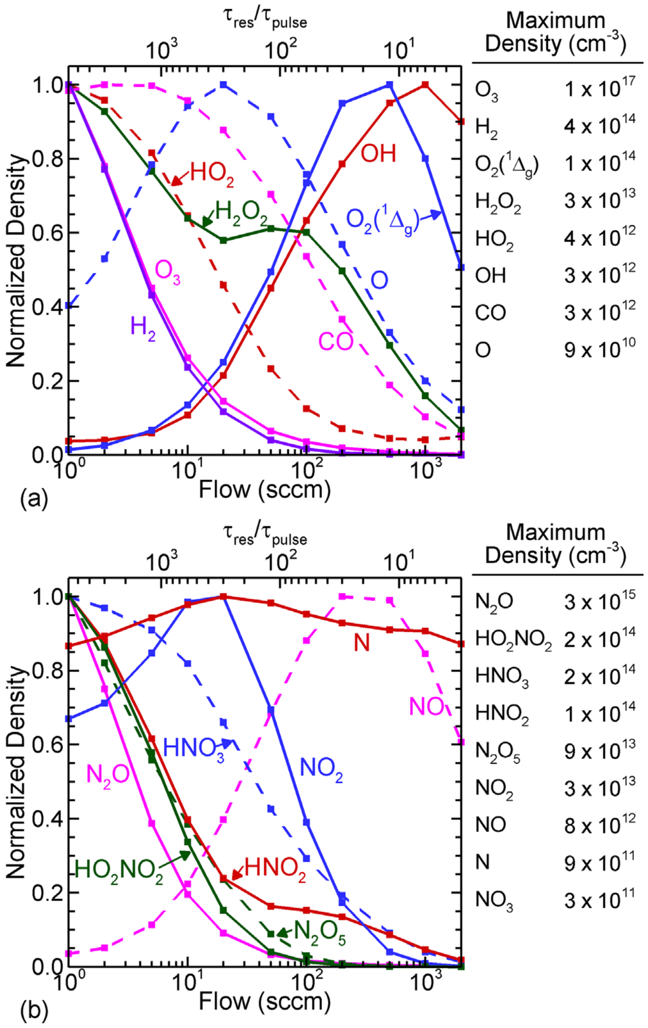

Figure 12. The densities of gas phase plasma produced RONS at the end of the last pulse (10 s) for different air flow rates. (a) ROS and (b) RNS. τ_r/τ_p is the average number of discharge pulses the average input gas molecule is exposed to before flowing out of the system. Values are shown normalized by their maximum density as a function of flow rate, shown to the right of each figure.

There are at least three ways in which flow can affect the reactive species densities in the gas at the end of the 5000 pulses. First, the evaporating water vapor into the gas phase is flushed out, so increasing flow decreases the relative humidity in the gas. Second, some of the reactive species flow out before they have time to undergo higher order reactions. Third, O_3 does not accumulate since it flows out the system which then prevents the previously discussed changes in the negative ion processes during later pulses.

Over the range of flow rates of 1–2000 sccm (τ_r/τ_p = 6000–3), the gas phase H_2O density varies from 8.6 × 10^{17} cm^{-3} to 1.3 × 10^{17} cm^{-3}. The air is less saturated with water vapor for shorter residence times. The peak electron density during the last pulse varies from 2.2 × 10^{12} cm^{-3} (flow rate of 1 sccm) to 2.4 × 10^{12} cm^{-3} (2000 sccm). This small increase in electron density is due to a combined effect of smaller densities of H_2O and O_3. The maximum value of T_e increases slightly as the humidity decreases with increasing flow rate, from 4.2 eV for 1 sccm to 4.3 eV for 2000 sccm, due to the decrease in H_2O. In short, as flow rates increase, O_3 and H_2O densities decrease, so n_e and T_e increase slightly. These small changes do not result in major changes in the initial production of reactants during the discharge pulse. The exceptions are those species

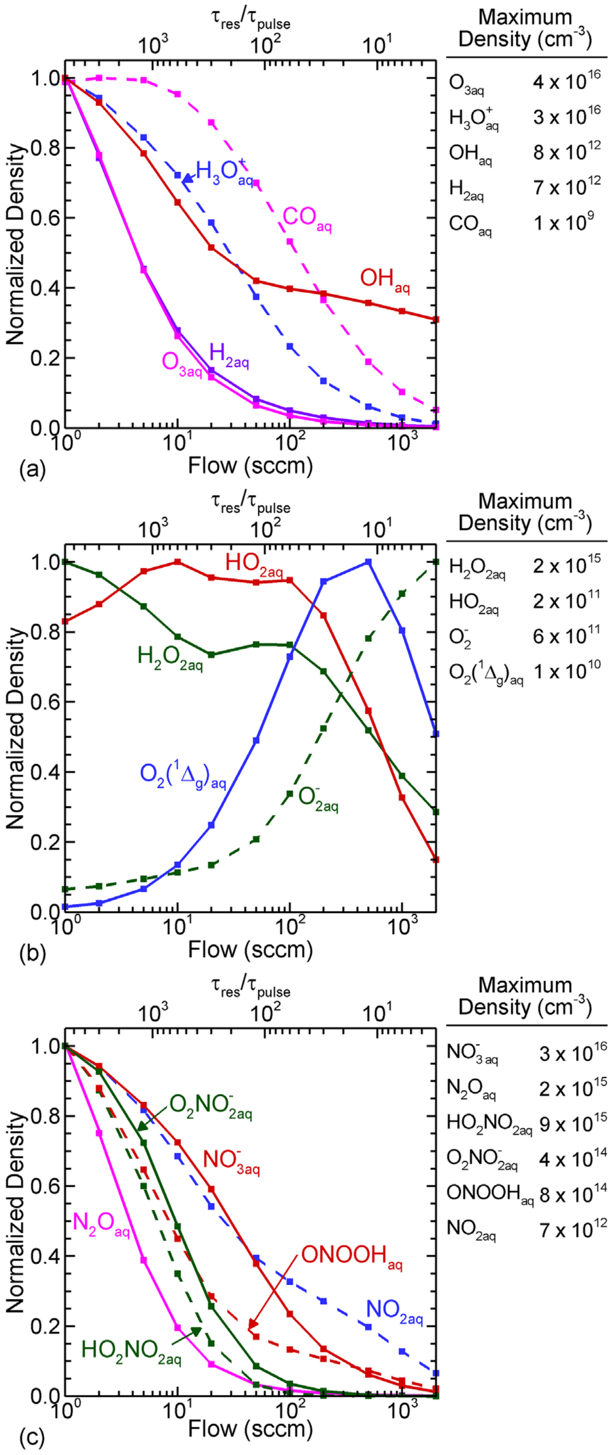

Figure 13. The densities of aqueous plasma produced reactive species at the end of the last pulse (10 s) for different air flow rates. (a) and (b) ROS and (c) RNS. τ_r/τ_p is the average number of discharge pulses the average input gas molecule is exposed to before flowing out of the system. Higher flow rates deliver more ROS than RNS to the liquid. Values are shown normalized by their maximum density as a function of flow rate, shown to the right of each figure.

whose production or consumption are dependent on the density of H_2O which decreases with increasing flow rate.

The gas phase RONS can be divided into three types of dependencies on flow rate. The densities of some species decrease with increasing flow rate simply because of a shorter residence time; the species or its precursors simply flow out of the system. There are also species whose densities decrease more gradually with flow rate because the RONS they react with also decrease with flow. Lastly, some species have a maximum density at an intermediate flow rate.

In the gas phase, O_3, H_2, N_2O, HO_2NO_4, N_2O_5 behave simply with flow rate—their densities decrease with increasing flow rate because their residence times decrease. This means there is less accumulation and, in the case of RNS, less opportunity for the multiple reactions required for their formation.

The second category of species, HNO_2, CO, HNO_3, HO_2 and H_2O_2, also decrease with increasing flow rate, however not as rapidly as the first group. For these species, there is some increase in their production as flow increases, but that increase in production is less significant than losses due to the increase in flow rate. The reactions which produce this slower decrease with flow include:

$$NO + OH + M \rightarrow HNO_2 + M, \tag{21a}$$

$$CO_2 + N \rightarrow CO + NO, \tag{21b}$$

$$OH + NO_2 + M \rightarrow HNO_3 + M. \tag{21c}$$

Each of these reactions have one or more reactants whose density increases with flow at some point in the range of 1–2000 sccm. For example, the density of HNO_2 decreases with flow but has a plateau between 20 sccm and 200 sccm. This range corresponds to a rapid increase in the density of NO (discussed below). For CO, the recombination with O_3 decreases as flow rate increases with there being less O_3, resulting in the density of CO decreasing more slowly with flow rate. The density of HO_2 also decreases more slowly with flow rate because its losses by the reaction $HO_2 + NO_2 + M \rightarrow HO_2NO_2 + M$ are also reduced.

As the flow rate increases, the density of H_2O_2 generally decreases. However at intermediate flow rates, 20 sccm–100 sccm, there is no decrease. The OH produced with each discharge pulse decreases with increasing flow rate, as the relative humidity decreases. However there are several reactions that can deplete OH after its production, including

$$OH + OH + M \rightarrow H_2O_2 + M, \tag{22a}$$

$$OH + NO_2 + M \rightarrow HNO_3 + M. \tag{22b}$$

As the flow rate increases, the density of NO_2 decreases, and so more of the OH generated during each pulse is available to produce H_2O_2. These opposing effects as flow rate increases cause the H_2O_2 density to stay approximately constant between 20 and 100 sccm.

The third category of gaseous species, which peak at an intermediate flow, includes $O_2(^1\Delta_g)$, OH, O, NO, and NO_2. The dependence of the densities of these species on flow rate should be evaluated not only in terms of their rates of production, but also in terms of how quickly they are consumed by reactions. The maximum rates of production of these species change very little with flow rate, but they are consumed by reactions more quickly at low flow rates due to there being larger densities of O_3 and NO_x. The dominant consuming reactions for each of these species are:

$$O_2(^1\Delta_g) + O_3 \rightarrow O_2 + O_2 + O, \tag{23a}$$

$$O + O_3 \rightarrow O_2(^1\Delta_g) + O_2, \tag{23b}$$

$$OH + O_3 \rightarrow HO_2 + O_2, \tag{23c}$$

$$NO + O_3 \rightarrow NO_2 + O_2, \tag{23d}$$

$$NO_2 + NO_3 + M \rightarrow N_2O_5 + M. \tag{23e}$$

These reactions occur on timescales on the order of the interpulse period and so their rates are not affected by flow out of the system until high flow rates. In general, the most stable gaseous RONS (O_3, H_2, N_2O, HO_2NO_4, N_2O_5, HNO_2, HO_2, CO, HNO_3, H_2O_2) decrease with increasing flow rate, while the species with a lifetime on the order of the interpulse period ($O_2(^1\Delta_g)$, OH, O, NO, and NO_2) peak at intermediate flow rates.

In this model, the liquid is well-stirred, but stagnant. That is, there is no convective flow as there is in the gas phase. Nevertheless, the composition of the liquid is a function of gas flow rate due to the rates of solvation of gas phase species. The dependence of the density of aqueous species on the gas phase flow rate is shown in figure 13. These dependencies can be separated into the same three groups: densities decreasing with flow due to residence time of gas phase species, decreasing with flow more slowly, and peaking at an intermediate flow rate.

The first category (aqueous densities decreasing with flowrates) includes all of the gas phase RNS, shown in figure 13(c), with the exception of NO_{2aq}. The RNS tend to take several reactions to form in the gas, and as a result, the gas phase RNS or their precursors leave the system at high flow rates before they can solvate into the liquid. O_{3aq}, H_{2aq}, and $H_3O^+_{aq}$ also simply decrease with flow rate due to a shorter residence time of their gas phase precursors.

The second category of species, densities which generally decrease with flow rate, include NO_{2aq}, H_2O_{2aq}, OH_{aq}, and CO_{aq}. The dependence of NO_{2aq} on flow rate differs from that of its gas phase precursor NO_2. At low flow rates when the densities of HO_2 and NO_2 are both high, the NO_2 can be stored in the cluster molecule HO_2NO_2, which then solvates in the liquid and produces NO_{2aq} at later times. At higher flow rates, the cluster molecule does not form in abundance, and the NO_{2aq} is mostly a result of direct solvation of NO_2. H_2O_{2aq} and CO_{aq} follow the dependence on gas phase flow rate of their gas phase precursors. The density of OH_{aq} decreases with flow rate until 50 sccm. Above 50 sccm, the density of OH_{aq} continues to decrease, but more slowly. This dependence differs from that of the density of gas phase OH because there are significant sources of OH_{aq} in the liquid, such as

$$O^-_{3aq} + H_3O^+_{aq} \rightarrow O_{2aq} + OH_{aq} + H_2O_{aq}, \tag{24a}$$

$$OH^-_{aq} + H_3O^+_{aq} \rightarrow H_{aq} + OH_{aq} + H_2O_{aq}, \tag{24b}$$

$$O_{aq} + H_2O_{aq} \rightarrow OH_{aq} + OH_{aq}, \tag{24c}$$

$$ONOOH_{aq} + H_2O_{aq} \rightarrow OH_{aq} + NO_{2aq} + H_2O_{aq}. \tag{24d}$$

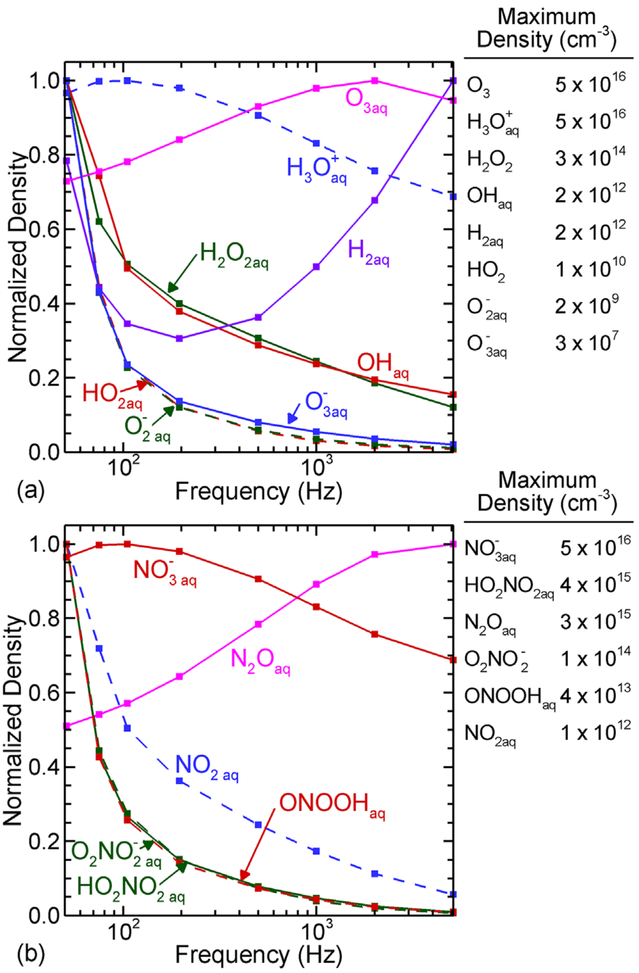

Figure 14. The densities of aqueous plasma produced reactive species at 110 s (relative to the beginning of the first pulse) for different pulse repetition frequencies. (a) ROS and (b) RNS. The reactive species decrease with PRF because for higher PRF it has been a longer time since the last voltage pulse. Values are shown normalized by their maximum density as a function of PRF, shown to the right of each figure.

These sources of OH_{aq} are more significant at low flow rates as there are higher densities of $ONOOH_{aq}$ and O^-_{3aq}. Above 50 sccm, the solvation of OH from the gas is the more significant source of OH_{aq}.

Liquid species whose densities are maximum at intermediate flow rates include $O_2(^1\Delta_g)_{aq}$, HO_{2aq}, and O^-_{2aq}. The variation of the density of $O_2(^1\Delta_g)_{aq}$ with flow rates simply matches the density of its gas phase precursor having a maximum at 500 sccm. HO_{2aq} hydrolyzes to form $H_3O^+_{aq}$ and O^-_{2aq} if the liquid is not too acidic. At higher flow rates the liquid is less acidic due to there being less solvated RNS. At flow rates above 100 sccm, the dissociated form of HO_{2aq} (O^-_{2aq}) dominates. The sum of the densities of HO_{2aq} and O^-_{2aq} monotonically increases with flow rate, which differs from the behavior of HO_2 in the gas. This sum increases with flow rate because OH_{aq} decreases with flow rate, and OH_{aq} consumes HO_{2aq} by the reaction $OH_{aq} + HO_{2aq} \rightarrow O_{2aq} + H_2O_{aq}$.

3.6. Pulse repetition frequency

When varying the pulse repetition frequency (PRF), comparing the reactive species densities at the end of the same number of pulses is misleading because species have had less time to react and solvate at high PRF. For this reason, we compared the reactive species as a function of PRF after 110 s, corresponding to 12 s after completing 5000 pulses at the lowest PRF. These results are shown in figure 14 for PRFs from 51 Hz to 5.1 kHz. The gas temperature is essentially 300 K at the lowest frequencies and reaches 307 K at 5.1 kHz. T_e is unaffected by PRF and the peak n_e decreases with PRF (from 2.9×10^{12} cm^{-3} to 2.4×10^{12} cm^{-3}).

The densities of most of the RONS, including OH_{aq}, H_2O_{2aq}, O^-_{3aq}, HO_{2aq}, O^-_{2aq}, $O_2NO^-_{2aq}$, $HO_2NO^-_{2aq}$, $ONOOH_{aq}$, and NO_{2aq} are strongly influenced by the time since the last voltage pulse. For the lowest frequency, 51 Hz, only 12 s have elapsed since the last discharge pulse and so most of the RONS have not yet decayed. For the highest frequency, 5.1 kHz, the time since the last pulse has been 109 s, and so more decay of the RONS has occurred. This trend is expected since, as shown in figure 7, most of the reactive densities decay in the afterglow.

The exceptions to this pattern are the most stable species—H_{2aq}, O_{3aq}, $H_3O^+_{aq}$, NO^-_{3aq}, N_2O_{aq}—whose densities do not monotonically decrease with increasing PRF. At higher PRF there is a greater tendency to form O_3, H_2, and N_2O, instead of HNO_3. A higher PRF means that the interpulse period is shorter than the diffusion time of gas phase species into the liquid and so gas phase reactions tend to dominate.

HNO_3 production is by $OH + NO_2 + M \rightarrow HNO_3 + M$, while the HNO_3 solvates with a large Henry's law constant. At high PRF, more NO_2 ends up in N_2O, rather than HNO_3, because the density of N is, on the average, higher for higher PRF

$$N + NO_2 \rightarrow N_2O + O. \quad (25)$$

In the end, this trend results in less production of HNO_3, and suggests that in an air plasma, PRF may be used to control the acidification of the liquid.

3.7. Biomolecules

In order to examine the consequences of biological molecules on the in liquid reactivity, peptidoglycan (PG) was added to the water. Peptidoglycan is the structural component of bacterial cell walls. Recent molecular dynamics (MD) simulations by Yusupov *et al* [42] have provided reaction probabilities for ROS with PG. The MD simulations did not include the mitigating effects of surrounding water molecules, so the reaction probabilities are likely an upper limit. The reaction rates used for the breaking of carbon–oxygen bonds (C–O), carbon–carbon bonds (C–C), and carbon–nitrogen bonds (C–N) are listed in table 3.

Table 3. Rate coefficients for reactions with peptidoglycan (cm^3 s^{-1}) [40].

Radical	C–O breaking	C–C breaking	C–N breaking
O_{aq}	6.35×10^{-10}	3.43×10^{-10}	3.96×10^{-10}
OH_{aq}	5.42×10^{-10}	2.92×10^{-10}	8.20×10^{-10}
O_{3aq}	4.80×10^{-10}	2.63×10^{-10}	4.74×10^{-10}
H_2O_{2aq}	2.32×10^{-10}	1.55×10^{-10}	—

The ROS in the liquid react with PG molecules that have not already reacted with RONS. The PG that does react is converted to a radical like form. Since PG is a large molecule, it is highly likely that the RONS will continue to react with the PG-radical. The initial concentration of PG in the liquid was chosen to be 100 ppm so that the PG was not depleted at the end of the simulation. The conditions are otherwise the same as the base case. Actual bio-relevant solutions may have a large range of densities of different biomolecules, and the biomolecules themselves will likely undergo very different reactions with in-liquid ROS. The goal of this parameterization is to emphasize the importance of the participation of biomolecules in the reaction mechanism. Reactions were only included for O_3, O, OH, and H_2O_2 with PG as those reaction probabilities were available, but reactions with RNS and HO_2 may also be significant. Since biological responses are complex and nonlinear, the amount of degradation of PG is not necessarily an indication of the potential of sterilization or killing of bacteria. However, this analysis provides insights into the importance of the consumption of RONS by organics to the gas and liquid phase chemistry.

Most of the densities of RONS, in both the gas and the liquid, as shown in figure 15, are lower with PG since PG consumes several radical species in these liquids. These processes correspond to a transfer of reactivity from the plasma produced species to the biological molecules. The end result is PG with broken bonds or radical sites, that could initiate a cascade of other reactions.

The PG influences the densities of reactive species in the gas by consuming their analogues in the liquid, whose replenishment may be limited by Henry's law saturation. Since the density of the species in the liquid is lowered by reaction with PG, the fluid can accept a larger fluence of this species from the gas during a given treatment time. This increase in the acceptance of gas phase species into the liquid is particularly true for O_3, which is at or near its Henry's law equilibrium value in the liquid for most of the plasma-on period. The maximum density of O_3 in the gas phase with PG (4.7×10^{15} cm^{-3}) is only 3% of the O_3 density in the base case (1.7×10^{17} cm^{-3}) without PG. O_{3aq} is largely depleted by reactions with PG, which then enables more O_3 from the gas phase to enter the liquid. In the base case, the buildup of O_3 decreases n_e by attachment towards the end of each plasma pulse. The final pulses with PG in the liquid have a slightly (4.7%) higher n_e in the gas phase than the base case because the density of O_3 is lower. This higher electron density during the later pulses results in an increased gas phase density of N, O, OH, and $O_2(^1\Delta_g)$. The density of H_2 in the gas is also higher with PG as a result of the reduced density of O_3. The production of H is higher with the higher n_e, and the H is more likely to combine into H_2 than undergo the reaction $H + O_3 \rightarrow OH + O_2$.

In the liquid, the species which react with PG (H_2O_{2aq}, OH_{aq}, O_{aq}, O_{3aq}) have lower densities than in the base case.

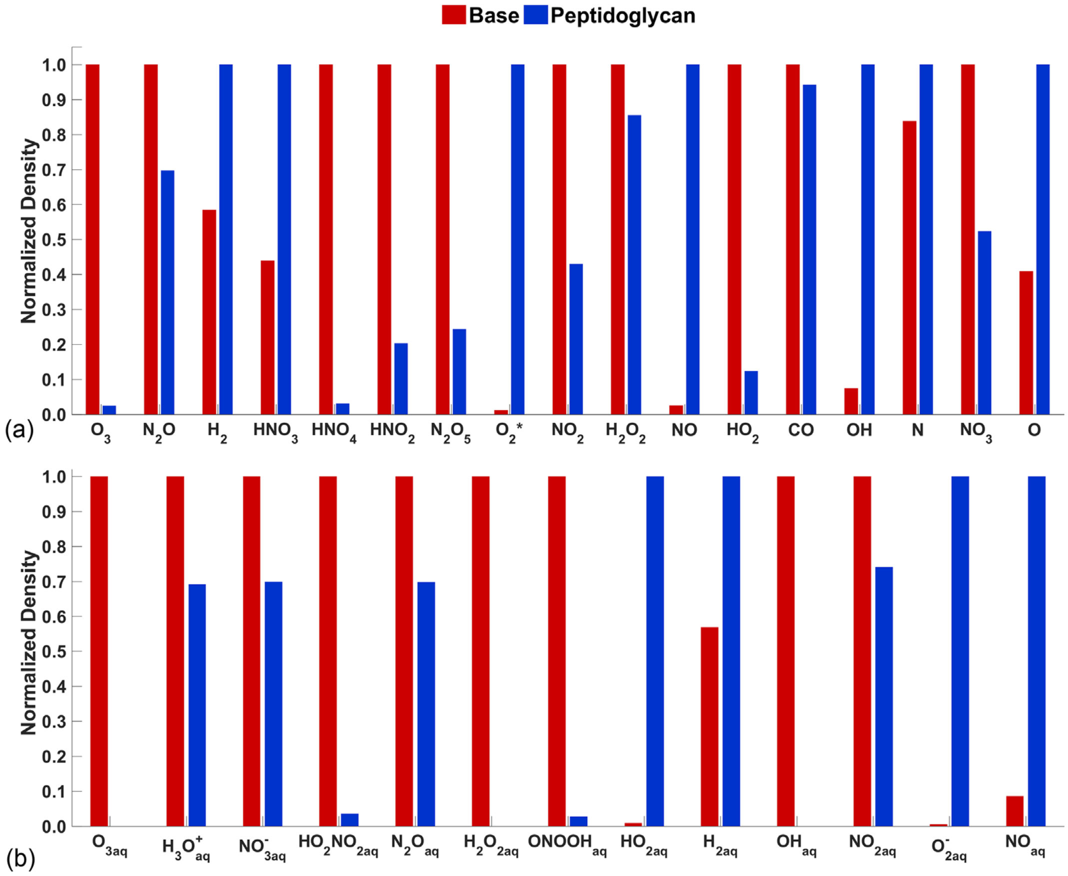

Figure 15. Densities of species in the (a) gas and (b) liquid after the 5000th discharge pulse (10 s) with and without peptidoglycan in the liquid. Species which directly react with PG in this mechanism include O, OH, O_3, and H_2O_2.

Most of the RONS densities in the liquid decrease with the addition of PG because the PG consumes several ROS important to their formation. Even though the RNS in the liquid do not directly react with the PG, they generally require ROS in their formation pathways and the ROS do react with PG. There are a few exceptions, however. The densities of HO_{2aq} and O^-_{2aq} are significantly larger with PG in the liquid. The density of HO_{2aq} is larger because it is not consumed by OH ($OH + HO_2 \rightarrow H_2O + O_2$), whose density decreases with the addition of PG. NO_{aq} is also higher, but recall that this is a short lived species, so its density is due to the last voltage pulse.

Although the production of HNO_3 in the gas is higher with PG, the density of its conjugate base NO^-_{3aq} is lower with PG. This is a result of the decrease in production of NO^-_{3aq} in the liquid from other radicals such as NO_{2aq} and NO_{3aq}. As a result, the liquid is less acidic with PG. The decrease in NO_2, NO_3, NO_{2aq}, NO_{3aq} and N_2O_{5aq} with PG also results in less $ONOOH_{aq}$ and HO_2NO_{2aq}.

In summary, the presence of organic molecules consumes much of the initial ROS reactivity, such as O_{aq}, OH_{aq}, and O_{3aq}, reducing the production of species which require many steps to form, such as HO_2NO_{2aq} and $ONOOH_{aq}$. The PG in the liquid also increases the fluence of ROS, especially O_3, that can be transferred from gas to the liquid over the treatment period.

4. Concluding remarks

Global modeling is a valuable method to address plasma–liquid interactions for long timescales with complete reaction mechanisms and without an unreasonable computational burden. This method is not suitable for addressing systems with unique geometrical dependencies, but is valuable to providing insights to systematic trends.

In an air DBD over liquid covered tissue, the positive ion dynamics are fairly consistent over several thousand discharge pulses. However, the negative ion dynamics evolve over thousands of pulses because of the accumulation of O_3 and NO_x which undergo attachment processes. Excited states and ions have lifetimes shorter than the interpulse period of 2 ms of the base case, but many more stable species accumulate with each pulse. In a well-stirred liquid, the rate of solvation of plasma produced species is a less sensitive function of their Henry's law constants than a system that is not well stirred due to the lack of a surface layer that may quickly saturate. However, at long enough time scales when equilibrium is fully established, these differences are less important. The dynamics of RONS in the liquid are pH dependent, as the dissociated and undissociated forms of weak acids undergo different reactions. O_{3aq} and NO^-_{3aq} are the most prevalent plasma produced liquid species and the nitric acid so formed lowers the final pH to 4.1 for the base case.

Increasing applied voltage generally increases the reactivity produced in the liquid, as the energy deposition is higher. Most of the species increase approximately linearly with applied voltage in both the gas and the liquid. The O_3 and the H_2 however, peak at an intermediate voltage. H_2 is dissociated as T_e increases with voltage, and O begins to react with larger densities of NO_2 instead of O_2 at higher voltages.

As the gas flow rate increases in an air DBD, the relative humidity decreases, and reactive but long lived species, including O_3, flow out of the system. Since O_3 and H_2O decrease with increasing flow rate, n_e and T_e increase. The densities of the most stable RNS decrease with flow rate, as they take several steps to form. Species with a lifetime on the order of the interpulse period peak at higher values of flow because there is not as much NO_x and O_3 in the gas for them to react with.

The presence of a biomolecule, peptidoglycan (PG) in the liquid reduces some of the accumulating effects in the liquid of previous pulses by consuming ozone. This is especially true for cases where the treatment time is longer than the time it takes for O_3 to solvate and react with a biomolecule. The reduction of density in the liquid of species that may otherwise be near their Henry's law equilibrium enables more of the species to solvate from the gas phase. Although reactions of RNS with the PG were not considered, the RNS in the liquid also decrease, as the ROS are precursors to RNS. This lower level of RONS in the liquid is a transfer of reactivity from the gas and liquid phase radical species to the biological system rather than a destruction of the reactivity.

Acknowledgments

This work was supported by the Department of Energy Office of Fusion Energy Science (DE-SC000319, DE-SC0014132), the National Science Foundation (PHY-1519117) and the NSF Graduate Research Fellowship Program.

References

[1] Arndt S *et al* 2013 *PLoS One* **8** e79325

[2] Kaushik N, Uddin N, Sim G B, Hong Y J, Baik K Y, Kim C H, Lee S J, Kaushik N K and Choi E H 2015 *Sci. Rep.* **5** 8587

[3] Daeschlein G *et al* 2014 *Plasma Process. Polym.* **11** 175

[4] Herrmann H W, Henins I, Park J and Selwyn G S 1999 *Phys. Plasmas* **6** 2284

[5] Edebo L, Holme T and Selin I 1968 *J. Gen. Microbiol.* **53** 1

[6] Graves D B 2014 *Clin. Plasma Med.* **2** 38

[7] Wegiel B, Hanto D W and Otterbein L E 2013 *Trends Mol. Med.* **19** 3

[8] Ray P D, Huang B W and Tsuji Y 2012 *Cell Signal* **24** 981

[9] Pagsberg P, Christensen H, Rabani J, Nilsson G, Fenger J and Nielsen S O 1969 *J. Phys. Chem.* **73** 1029

[10] Lukes P, Dolezalova E, Sisrova I and Clupek M 2014 *Plasma Sources Sci. Technol.* **23** 015019

[11] Traylor M J, Pavlovich M J, Karim S, Hait P, Sakiyama Y, Clark D S and Graves D B 2011 *J. Phys. D. Appl. Phys.* **44** 472001

[12] Tresp H, Hammer M U, Weltmann K and Reuter S 2013 *Plasma Med.* **3** 45

[13] Foster J E, Adamovsky G, Gucker S N and Blankson I M 2013 *IEEE Trans. Plasma Sci.* **41** 503

[14] Rumbach P, Bartels D M, Sankaran R M and Go D B 2015 *Nat. Commun.* **6** 7248

[15] Tresp H, Hammer M U, Winter J, Weltmann K-D and Reuter S 2013 *J. Phys. D. Appl. Phys.* **46** 435401

[16] Ognier S, Iya-Sou D, Fourmond C and Cavadias S 2009 *Plasma Chem. Plasma Process.* **29** 261

[17] Matsui Y, Takeuchi N, Sasaki K, Hayashi R and Yasuoka K 2011 *Plasma Sources Sci. Technol.* **20** 034015

[18] Takeuchi N, Ishii Y and Yasuoka K 2012 *Plasma Sources Sci. Technol.* **21** 015006

[19] Kelly S and Turner M M 2014 *Plasma Sources Sci. Technol.* **23** 065012

[20] Liu Z C, Liu D X, Chen C, Li D, Yang A J, Rong M Z, Chen H L and Kong M G 2015 *J. Phys. D. Appl. Phys.* **48** 495201

[21] Beebe S J, Blackmore P F, White J, Joshi R P and Schoenbach K H 2004 *Physiol. Meas.* **25** 1077

[22] Dorai R and Kushner M J 2002 *J. Phys. D. Appl. Phys.* **35** 2954

[23] van Rens J F M, Schoof J T, Ummelen F C, van Vugt D C, Bruggeman P J and van Veldhuizen E M 2014 *IEEE Trans. Plasma Sci.* **42** 2622

[24] Rumbach P, Griggs N, Sankaran R M and Go D B 2014 *IEEE Trans. Plasma Sci.* **42** 2610

[25] Sander R 2015 Compilation of Henry's law constants (version 4.0) for water as solvent *Atmos. Chem. Phys.* **15** 4399

[26] Van Gaens W and Bogaerts A 2014 *Plasma Sources Sci. Technol.* **23** 035015

[27] Tian W and Kushner M J 2014 *J. Phys. D. Appl. Phys.* **47** 165201

[28] Madden K P and Mezyk S P 2011 *J. Phys. Chem. Ref. Data* **40** 023103

[29] NDRL/NIST Solution Kinetics Database (available at http://kinetics.nist.gov/solution/)

[30] NIST Chemical Kinetics Database (available at http://kinetics.nist.gov/kinetics/)

[31] Person J C and Ham D O 1988 *Radiat. Phys. Chem.* **31** 1

[32] Atkinson R, Baulch D L, Cox R A, Crowley J N, Hampson R F, Hynes R G, Jenkin M E, Rossi M J and Troe J 2003 *Atmos. Chem. Phys.* **3** 6179

[33] Pandis S N and Seinfeld J H 1989 *J. Geophys. Res.* **94** 1105

[34] Kossyi I A, Kostinsky A Y, Matveyev A A and Silakov V P 1992 *Plasma Sources Sci. Technol.* **1** 207

[35] Lieberman M A and Lichtenberg A J 2005 *Principles of Plasma Discharges and Materials Processing* (New York: Wiley) p 273

[36] Lepoutre F, Louis G and Manceau I I 1977 *Chem. Phys. Lett.* **48** 3

[37] Graven W M and Long F J 1954 *J. Am. Chem. Soc.* **76** 2602

[38] Große-Kreul S, Hübner S, Schneider S, Ellerweg D, von Keudell A, Matejčík S and Benedikt J 2015 *Plasma Sources Sci. Technol.* **24** 044008

[39] van Gils C A J, Hofmann S, Boekema B K H L, Brandenburg R and Bruggeman P J 2013 *J. Phys. D. Appl. Phys.* **46** 175203

[40] Ding K and Lieberman M A 2015 *J. Phys. D. Appl. Phys.* **48** 035401

[41] Guerra V, Sá P A and Loureiro J 2001 *J. Phys. D. Appl. Phys.* **34** 1745

[42] Yusupov M, Bogaerts A, Huygh S, Snoeckx R, van Duin A C T and Neyts E C 2013 *J. Phys. Chem.* C **117** 5993